International Mathematical Forum, 3, 2008, no. 42, 2049 - 2079

A Lagrangian Approach to Two-Dimensional Free Surface Flows

Giorgio Riccardi and Danilo Durante

Dept. of Aerospace and Mechanical Engineering
II University of Naples, via Roma, 29-81031 Aversa (Ce), Italy
giorgio.riccardi@unina2.it, danilo.durante@unina2.it

Abstract

The two-dimensional, free surface motion of an inviscid isochoric fluid is investigated, through a lagrangian approach. Among the equations of motion, a pressure equation is also considered. It is deduced from the continuity constraint, in analogy with the classical eulerian formulation for isochoric fluids.

The flow is numerically simulated by using standard finite differences, with staggered pressure and a predictor-corrector time integration scheme. The continuity constraint is directly enforced in the corrector substep.

Moreover, a small perturbation analysis is performed, in order to obtain an approximated analytical solution of the lagrangian equations. The perturbation parameter is related to the amplitude of the initial velocity field. The expansion is carried out up to second order terms, accounting for metrical coefficients and the source term in the pressure equation. In presence of a gravitational field, the free surface elevation results a time periodic one in the first order solution, while the periodicity is lost at second order. The flow as a whole is not a time periodic one. Comparisons with the direct numerical simulation of the flow are discussed.

Mathematics Subject Classification: 76B15, 76M20

Keywords: $2D$ free surface flows, lagrangian approach, gravity water waves

1 Introduction

The present paper deals with an analytical and numerical study of the motion of an isochoric and inviscid fluid, in presence of a free surface. The analysis is

restricted to small displacements of the free surface, so that a full lagrangian approach appears to be natural, although "... it is seldom used in modern fluid dynamics" [8]. For an inviscid fluid, the reasons are related to the more complex form of the pressure equation, in which metrical terms appear, and to the difficulties in enforcing volume conservation. As a matter of fact, this constraint becomes a nonlinear one in a lagrangian framework.

A lagrangian description of the free surface was indeed adopted in the fundamental work of Longuet-Higgins and Cokelet [3], where a mixed eulerian-lagrangian approach has been proposed. In order to evaluate free surface velocities, the mixed approach employs also an eulerian description of the flow field, based on boundary integral equations [5] or finite differences, or finite elements [2]. The mixed approach made it possible to analyze flows with large free surface deformations, opening the way to the accurate computation and so to the physical understanding of overturning waves.

In 1998 a quite different approach has been proposed, which appears to be closer to a full lagrangian description of the flow. Protopopov [6] used a mixed approach, in which the motion of a lagrangian grid is also followed. The results appear quite attractive, especially for the computation of overturning waves.

Recently, the lagrangian hydrodynamics framework has been extended through a new formulation of the classical equations of motion [8], which focuses on the Jacobi matrix of the flow. The *matrix approach* appears to be more elegant than the classical one (see [4], for example) and analytical solutions become also possible, even for rather complex three-dimensional flow fields.

In the present paper, the lagrangian equations of motion are written in Section 2, by transforming the standard Euler equations for an isochoric fluid. The resulting formulation is put in a compact form through the Jacobi matrix of the flow. In Section 3, a discrete scheme for the numerical integration of such equations is briefly described.

At the same time, the solution of the lagrangian equations of motion is approached also from an analytical point of view, through a small perturbation expansion (see Section 4), carried out up to second order terms. The basic hypothesis is that the displacement of each fluid particle from its initial position remains small, compared with an overall scale of the flowfield. For this reason, the perturbation parameter is related to the amplitude of the initial velocity field and small times are considered.

Solutions are almost periodic in presence of a gravitational field, while they are monotonic in absence of gravity. Comparisons with the results of numerical simulations are discussed in Section 5. Conclusions are offered in Section 6, together with a short description of the future work on a conformal mapping in lagrangian coordinates.

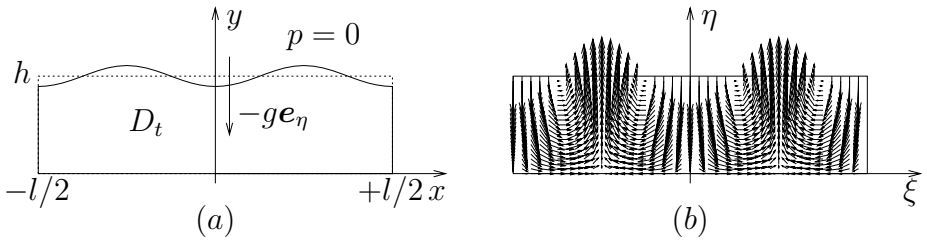

Figure 1: In (a) a sketch of the fluid domain D_t (∂D_0 is also drawn with dashed line) is shown. $\boldsymbol{e}_\eta$ is the unit vector along the η axis. A sample of initial conditions on particle positions and velocities is drawn in (b).

2 Lagrangian equations of motion

The two-dimensional flow in a periodic domain is considered, as shown in Fig. 1-a. An inviscid and isochoric fluid lies at the initial time ($t = 0$) in a rectangular domain (length l and height h). The free surface is the top horizontal side, while the bottom one is a solid wall. Moreover, on the two vertical sides (at $\xi = \pm l/2$), periodical conditions are imposed (hereafter, they are implicitly considered). As a consequence, the eulerian description of the motion poses the following problem: [1]

$$\begin{cases} \dfrac{D\boldsymbol{u}}{Dt} = -\boldsymbol{\nabla}_e P \\ \nabla_e^2 P = -(u_x^2 + 2u_y v_x + v_y^2) \\ \partial_y P = 0 \quad \text{on the bottom wall,} \quad P = gy \quad \text{on the free surface .} \end{cases} \tag{1}$$

In equation (1), $\boldsymbol{\nabla}_e = (\partial_x, \partial_y)$, D/Dt stays for the material time derivative, $\boldsymbol{u} = (u, v)$ is the velocity and $P = p + g\,y$, where p is the pressure (divided by the fluid density) and g is the gravitational acceleration ($g > 0$, see Fig. 1-a). Hereafter, suffixes (like "x" in "u_x") indicate partial derivatives (of "u" with respect to "x").

In the eulerian description of the flow, the system (1) is integrated in the fluid domain D_t, see Fig. 1-a, whose shape depends, in turn, on the solution itself. As usually, the incompressibility constraint $\boldsymbol{\nabla}_e \cdot \boldsymbol{u} = 0$ has been employed, in order to derive the pressure equation. The boundary condition on the pressure on the bottom wall follows from the impermeability constraint $v \equiv 0$, while on the free surface $p = 0$ is enforced, see Fig. 1-a.

In the present section, the above equations are transformed by the lagrangian map $\boldsymbol{\xi} = (\xi, \eta) \mapsto \boldsymbol{x} = (x, y)$, obtaining a differential system in terms

[1] Vectors, matrices or complex numbers will be written with bold symbols.

of $\boldsymbol{x}$, $\boldsymbol{u} = \dot{\boldsymbol{x}}$ ($\dot{\boldsymbol{x}}$ stays for time derivative of $\boldsymbol{x}$) and P. The equations of motion will be written in matrix form, through the Jacobi matrix of the flow:

$$\boldsymbol{G} = \begin{pmatrix} x_\xi & y_\xi \\ x_\eta & y_\eta \end{pmatrix} \tag{2}$$

(note that this matrix is the transposed of the usual Jacobi matrix). The continuity constraint, together with the initial conditions:

$$\boldsymbol{x}(\boldsymbol{\xi}; 0) = \boldsymbol{\xi} \,, \tag{3}$$

imply that the matrix (2) has a unitary determinant:

$$\mathcal{G} = |\boldsymbol{G}| = x_\xi \, y_\eta - x_\eta \, y_\xi \equiv 1 \,, \tag{4}$$

for any lagrangan position $\boldsymbol{\xi}$ and time t.

In order to write the lagrangian equations of motion, the eulerian operators $\boldsymbol{\nabla}_e$ and ∇_e^2 are written in lagrangian form:

$$\begin{aligned} \boldsymbol{\nabla}_e &\mapsto \boldsymbol{G}^{-1} \cdot \boldsymbol{\nabla} = (y_\eta \partial_\xi - y_\xi \partial_\eta, -x_\eta \partial_\xi + x_\xi \partial_\eta) \\ \nabla_e^2 &\mapsto \mathcal{L} = (\boldsymbol{G}^{-1} \cdot \boldsymbol{\nabla}) \cdot (\boldsymbol{G}^{-1} \cdot \boldsymbol{\nabla}) \\ &\qquad = N^2 \, \partial^2_{\xi\xi} - 2 \, S \, \partial^2_{\xi\eta} + M^2 \, \partial^2_{\eta\eta} + Q \, \partial_\xi + R \, \partial_\eta \,, \end{aligned} \tag{5}$$

where $\boldsymbol{\nabla} = (\partial_\xi, \partial_\eta)$ and M, N, $S = MN \cos\phi$, Q and R are the metrical coefficients: [2]

$$\begin{aligned} &M^2 = |\boldsymbol{x}_\xi|^2 \,, \;\; S = \boldsymbol{x}_\xi \cdot \boldsymbol{x}_\eta \,, \;\; N^2 = |\boldsymbol{x}_\eta|^2 \\ &Q = \partial_\xi N^2 - \partial_\eta S \,, \;\; R = \partial_\eta M^2 - \partial_\xi S \,. \end{aligned} \tag{6}$$

Note that, from the identity $M^2 N^2 - S^2 \equiv 1$, $|\sin\phi| = 1/(MN)$ follows. By using the lagrangian forms (5) of the differential operators $\boldsymbol{\nabla}_e$ and ∇_e^2, the differential system (1) becomes:

$$\begin{cases} \dot{\boldsymbol{x}} = \boldsymbol{u} \\ \dot{\boldsymbol{u}} = -\boldsymbol{G}^{-1} \cdot \boldsymbol{\nabla} P \\ \mathcal{L} \, P = (\dot{\boldsymbol{G}}^{-1} \cdot \boldsymbol{\nabla}) \cdot \boldsymbol{u} = 2 \, |\dot{\boldsymbol{G}}| \\ -x_\eta P_\xi + x_\xi P_\eta = 0 \quad \text{for } \eta = 0, \quad P = gy \quad \text{for } \eta = h. \end{cases} \tag{7}$$

[2] It is worth noticing that $\mathcal{L}$ is still elliptical, *for any flow*. As a matter of fact, the eigenvalues $\lambda_{1,2}$ of the matrix of the coefficients of the second order derivatives in $\mathcal{L}$ are:

$$\lambda_{1,2} = (M^2 + N^2) \left(1 \pm \sqrt{1 - \delta^2 \sin^2 \phi} \, \right) / 2 \,,$$

with $\delta = 2MN/(M^2 + N^2) \leq 1$. It follows that λ_1 and λ_2 are both positive.

In order to write the pressure equation in the problem (7), a more physical way lies in enforcing $\ddot{\mathcal{G}} = 0$. As a matter of fact, this condition implies that $\mathcal{G}$ remains unitary for any $\boldsymbol{\xi}$ and t, being $\mathcal{G} \equiv 1$ and $\dot{\mathcal{G}} = \boldsymbol{\nabla}_e \cdot \boldsymbol{u} \equiv 0$ at $t = 0$. In the following, the system (7) is considered in a non dimensional form. The length scale is l (which is also the period in ξ of the solution), while a suitable velocity scale follows from the initial velocity field, see equation (8) below.

The lagrangian description of the flow is obtained by integrating the system (7), with proper initial conditions on particle positions $\boldsymbol{x}(\boldsymbol{\xi}; 0)$ and velocities $\boldsymbol{u}(\boldsymbol{\xi}; 0)$, see Fig. 1-*b*. In the present paper, the integration of the system (7) is carried out through numerical simulations and a small perturbation analysis. A discrete scheme for the numerical simulation of the solution of the system (7) is briefly described in the next section, while Section 4 is devoted to the analytical approach.

3 Numerical algorithm

Numerical simulations of the solution of the system (7) are performed, through standard second order finite differences with staggered pressure. By indicating with superscripts ^{n} (subscripts for the Jacobi matrix) quantities at the time t^n, the following fractional-step time integration scheme ($\Delta t_2 = \Delta t/2$, periodical conditions omitted) is adopted:

predictor substep:

$$\begin{cases} (\boldsymbol{G}_n^{-1} \cdot \boldsymbol{\nabla}) \cdot (\boldsymbol{G}_n^{-1} \cdot \boldsymbol{\nabla}) P^n = (\dot{\boldsymbol{G}}_n^{-1} \cdot \boldsymbol{\nabla}) \cdot \boldsymbol{u}^n \\ -x_\eta^n P_\xi^n + x_\xi^n P_\eta^n = 0 \quad \text{for } \eta = 0, \quad P^n = g\, y^n \quad \text{for } \eta = h \end{cases}$$

$$\boldsymbol{x}^{n+1/2} = \boldsymbol{x}^n + \Delta t_2\, \boldsymbol{u}^n$$

$$\boldsymbol{u}^{n+1/2} = \boldsymbol{u}^n - \Delta t_2\, \boldsymbol{G}_n^{-1} \cdot \boldsymbol{\nabla} P^n$$

corrector substep:

$$\begin{cases} \quad [(\boldsymbol{G}_{n+1/2}^{-1} + \Delta t\, \dot{\boldsymbol{G}}_{n+1/2}^{-1} - \Delta t_2\, \dot{\boldsymbol{G}}_n^{-1}) \cdot \boldsymbol{\nabla}] \cdot (\boldsymbol{G}_{n+1/2}^{-1} \cdot \boldsymbol{\nabla}) P^{n+1/2} = \\ = (\dot{\boldsymbol{G}}_{n+1/2}^{-1} \cdot \boldsymbol{\nabla}) \cdot \boldsymbol{u}^n \\ -x_\eta^{n+1/2} P_\xi^{n+1/2} + x_\xi^{n+1/2} P_\eta^{n+1/2} = 0 \quad \text{for } \eta = 0, \\ P^{n+1/2} = g\, y^{n+1/2} \quad \text{for } \eta = h \end{cases}$$

$$\boldsymbol{x}^{n+1} = \boldsymbol{x}^n + \Delta t\, \boldsymbol{u}^{n+1/2}$$

$$\boldsymbol{u}^{n+1} = \boldsymbol{u}^n - \Delta t\, \boldsymbol{G}_{n+1/2}^{-1} \cdot \boldsymbol{\nabla} P^{n+1/2}\,.$$

The pressure $P^{n+1/2}$ is evaluated by imposing that $\boldsymbol{u}^{n+1}$ is divergence-free: $(\boldsymbol{G}_{n+1}^{-1} \cdot \boldsymbol{\nabla}) \cdot \boldsymbol{u}^{n+1} = 0$ where, due to the linearity of $\boldsymbol{G}^{-1}$ in $\boldsymbol{x}$, the following

relations hold: [3]

$$\boldsymbol{G}_{n+1/2}^{-1} = \boldsymbol{G}_n^{-1} + \Delta t_2 \, \dot{\boldsymbol{G}}_n^{-1} \ , \ \ \boldsymbol{G}_{n+1}^{-1} = \boldsymbol{G}_{n+1/2}^{-1} + \Delta t \, \dot{\boldsymbol{G}}_{n+1/2}^{-1} - \Delta t_2 \, \dot{\boldsymbol{G}}_n^{-1} \ .$$

The explicit form of the pressure equation in the corrector substep is written in Appendix A.

The predictor substep starts with the evaluation of the pressure P^n at time t^n, then positions and velocities are upgraded ($\boldsymbol{x}^{n+1/2}$, $\boldsymbol{u}^{n+1/2}$) by using such pressure. The corrector substep begins with the pressure calculation ($P^{n+1/2}$), from which the new positions $\boldsymbol{x}^{n+1}$ and velocities $\boldsymbol{u}^{n+1}$ at time t^{n+1} are obtained. The pressure problems are solved with the Gauss-Seidel iterative method, which is stopped when the discrete L_2 norm of the residual is lower that a fixed threshold (10^{-10} in the present calculations).

3.1 Analysis of numerical results in a sample case

The numerical simulation has been carried out for an initial velocity field of the form (α and β are positive integers):

$$U = \sin\left(2\,\pi\,\alpha\,\frac{\xi}{l}\right)\cos\left(\frac{\pi}{2}\,\beta\,\frac{\eta}{h}\right) \ , \quad V = \rho\,\cos\left(2\,\pi\,\alpha\,\frac{\xi}{l}\right)\sin\left(\frac{\pi}{2}\,\beta\,\frac{\eta}{h}\right) \ , \tag{8}$$

where $\rho = -4\,(\alpha h)/(\beta l)$, $\boldsymbol{U} = U + \mathrm{i}V$ ($\mathrm{i} = \sqrt{-1}$) being divergence-free. In a Fourier expansion along ξ, the integer α identifies the two modes (at wavenumbers $\pm 2\pi\alpha/l$), which are directly excited by the initial data.

The numerical simulations are carried out by setting the initial conditions in the following form:

$$\boldsymbol{x}(\boldsymbol{\xi};0) = \boldsymbol{\xi} \ , \ \ \boldsymbol{u}(\boldsymbol{\xi};0) = \dot{\boldsymbol{x}}(\boldsymbol{\xi};0) = \varepsilon\,\boldsymbol{U}(\boldsymbol{\xi}) \ , \tag{9}$$

where ε is a fixed (small) positive number. ε will be employed as perturbation parameter in the next section.

In Fig. 2 computational grids, isobars (*i.e.*, the isolines of the pressure $P - gh = p + g(y - h)$, which vanishes on the free surface at $t = 0$) and free surface accelerations are shown at several times. $\alpha = 2$ is used, so that the mode 2 is excited by the initial conditions, while all the other modes will be excited by nonlinearities (metrical terms and the source term in the pressure equation). An analytical solution of the system (7), which will be addressed in Section 4, exhibits a time periodic behaviour of the elevation of the free surface, whose period (T_α, in the following) is a decreasing function of α. The present simulation is carried out during the first "period" of oscillation (T_2,

[3] Here, $\dot{\boldsymbol{G}}^{-1}$ stays for the time derivative of $\boldsymbol{G}^{-1}$, which is different from the inverse matrix of $\dot{\boldsymbol{G}}$.

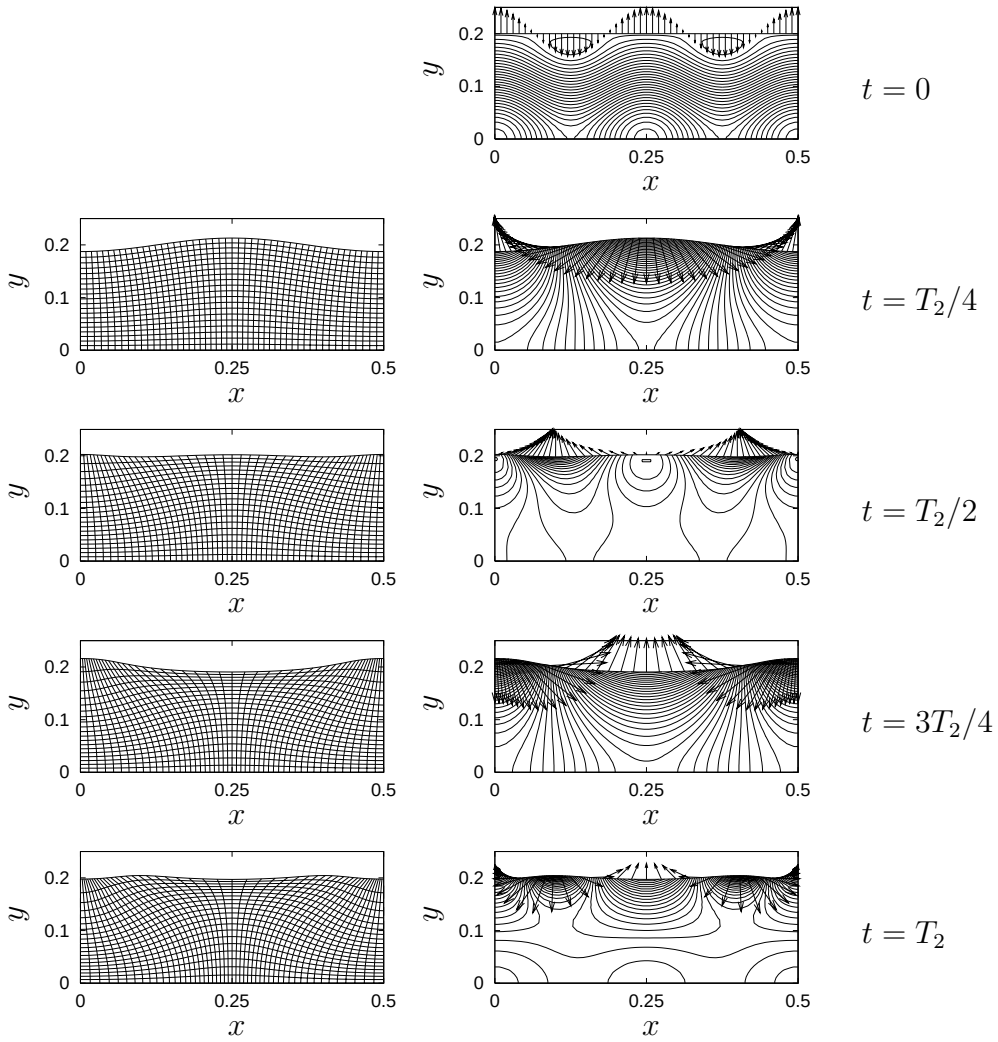

Figure 2: From the top to the bottom, computational grids (on the left), isobars and free surface accelerations (on the right) during the period $T_2 \simeq 2.523$, for the flow with $h = 0.2$ and $g = 0.5$. The initial velocity field has the form (8), with $\varepsilon = 0.02$, $\alpha = 2$ and $\beta = 1$. The pressure isolines are drawn with steps $\Delta P = 2 \cdot 10^{-5}$ at $t = 0$, $2 \cdot 10^{-4}$ at times $T_2/4$ and $3T_2/4$, 10^{-4} at times $T_2/2$ and T_2. Free surface accelerations are drawn with a scale of 20 at $t = 0$ and with a unitary scale at other times. A 101×21 grid is employed, with time step $\Delta t = T_2/800$.

say) of the free surface, with an error $|D_{T_2}|/|D_0| - 1 \simeq 4.097 \cdot 10^{-4}$ on the area $|D_t|$ of the fluid domain.

Numerical results are shown at four times, which correspond to extreme positions of the free surface ($t = T_2/4,\ 3T_2/4$) and to configurations with a flat surface ($t = T_2/2,\ T_2$) in the framework of the analytical solution. The pressure field at $t = 0$ has negative minima near the free surface, on which it vanishes. Moreover, it exhibits a monotone growth from the free surface to the bottom wall, where it reaches its maxima. Being the Jacobi matrix of the flow a unitary one at $t = 0$, the accelerations are just $-\boldsymbol{\nabla} P$. As a consequence, they are outward in the region in which the pressure grows just below the surface and inward in the regions in which the pressure diminishes. Note that the intensities are rather small. At time $T_2/4$, both maximum (at $x = 0.25$) and minima (at $x = 0$ and 0.5) intensify and reach the free surface. As before, the free surface accelerations are roughly directed along $-\boldsymbol{\nabla} P$, but their intensities grow more than a factor 20. At time $T_2/2$, the pressure field is almost flat: there are three maxima just below the free surface (at $x = 0$, 0.25 and 0.5) and two minima on the surface itself. As a result, all the accelerations are outward. At time $3T_2/4$, two maxima (at $x = 0$ and 0.5) and one minimum (at $x = 0$) are present on the free surface. This is just the opposite configuration, with respect to the one at time $T_2/4$. At time T_2, three minima (at $x = 0$, 0.25 and 0.5) and two maxima are present on the free surface, while three maxima are located on the bottom wall. This is roughly the opposite configuration with respect to the one at time $T_2/2$, moreover it is in a qualitative agreement with the configuration at the initial time.

The analysis of the motion in terms of the lagrangian positions, shown in the left column of Fig. 2, is simplified by considering Fourier's coefficients along ξ for x and y coordinates:

$$\boldsymbol{x}_m(\eta;t) = \frac{1}{l}\int_0^l d\xi\, x(\xi,\eta;t)\, e^{-\mathrm{i}\mathrm{M}\xi}\ ,\ \ \boldsymbol{y}_m(\eta;t) = \frac{1}{l}\int_0^l d\xi\, y(\xi,\eta;t)\, e^{-\mathrm{i}\mathrm{M}\xi} \qquad (10)$$

(m is a relative integer and $\mathrm{M} = 2\pi m/l$ is the corresponding wavenumber). At each time, they are evaluated through a numerical integration with a second order formula, while they hold $\boldsymbol{x}_m(\eta;0) \equiv \mathrm{i}(-1)^m/\mathrm{M}$ and $\boldsymbol{y}_m(\eta;0) \equiv 0$ at the initial time, see Section 4. For the times under consideration, the real parts of Fourier's coefficients for x vanish, while the same occurs for the imaginary parts of the coefficients for y. It means that Fourier's series for x is a sine series, while the corresponding one for y is a cosine series.

Fourier's coefficients are shown in Fig. 3 vs. η for $m = 2,\ 4,\ 6$ and at the four times $t = T_2/4,\ T_2/2,\ 3T_2/4$ and T_2. For the three wavenumbers investigated, deformations of the computational grid appear to be more intense [4] along x, than along y. The mode 2 is related to x-displacements

[4] It is worth noticing that the x-deformations have to be calculated accounting for the

which are proportional to $+\sin 4\pi\xi$ near the wall, where the imaginary part of $\boldsymbol{x}_2(\eta;t)-\boldsymbol{x}_2(\eta;0)$ is negative. On the contrary, for $\eta > h/2$ the x-displacements become proportional to $-\sin 4\pi\xi$, reaching their maximum amplitude on the free surface. The y-displacement is always proportional to $-\cos 4\pi\xi$, with the exception of a neighbourhood of the free surface at $t = 3T_2/4$. At the initial time, the larger y-displacement is reached on the free surface, while at later times it is reached roughly for $\eta = 0.5$. With the first order analytical expansion of Section 4, these modes are quite well approximated, as it will be discussed in Section 5.

The mode 4 is significant because it is the first induced by non-linear terms and not directly excited by the initial conditions. The related x-displacements have amplitudes at least 7 times smaller than the one of the mode 2, while the y-displacements are 10 times smaller and reach their maximum just below the free surface. It is worth noticing that for the first half period mode 4 remains very close to its initial value: nonlinear interactions take this time to excite such mode. With the second order analytical expansion of Section 4, mode 4 is quite well approximated, at least for $0 < t < T_2/2$, while larger errors appear at later times, due to the excitation of mode 6. This latter one is shown in the third row of Fig. 3. It reach significant values only in the second half of the examined time period and cannot be followed by the analytical solution.

In the present paper the solution of the lagrangian system (7) is addressed also from an analytical point of view, through a small perturbation approach, in the main hypothesis that the displacement of each particle from its initial position is negligible with respect to the characteristic lengths of the fluid domain (*i.e.*, l and h). The following section is devoted to this analysis.

4 Small perturbation solution for the flow

In the present section, a flow $\boldsymbol{x}(\boldsymbol{\xi};t)$ in which each fluid particle moves of a small displacement from its initial position $\boldsymbol{\xi}$ is considered. To this aim, the initial velocity field $\boldsymbol{u}(\boldsymbol{\xi};0) = u(\xi,\eta;0) + \mathrm{i}\, v(\xi,\eta;0)$ is assigned as in equation (9), where the divergence-free field $\boldsymbol{U} = U + \mathrm{i}\, V$ is assumed of the order of the unity, together with all its derivatives, and ε is a positive, small parameter. It is required that $U(\pm l/2,\eta) \equiv 0$ and that $U(\xi,\eta)$ has a vanishing mean value in ξ, for any η.

All the fields in the system (7) are assumed to be smooth functions of the parameter ε. They are expanded in McLaurin's series of ε, for example the flow itself is expanded as:

$$\boldsymbol{x}(\boldsymbol{\xi};t) = \boldsymbol{\xi} + \varepsilon\, \boldsymbol{x}^{(1)}(\boldsymbol{\xi};t) + \varepsilon^2\, \boldsymbol{x}^{(2)}(\boldsymbol{\xi};t) + \dots\,, \tag{11}$$

nonvanishing Fourier's coefficients $\boldsymbol{x}_m(\eta;0)$ at the initial time.

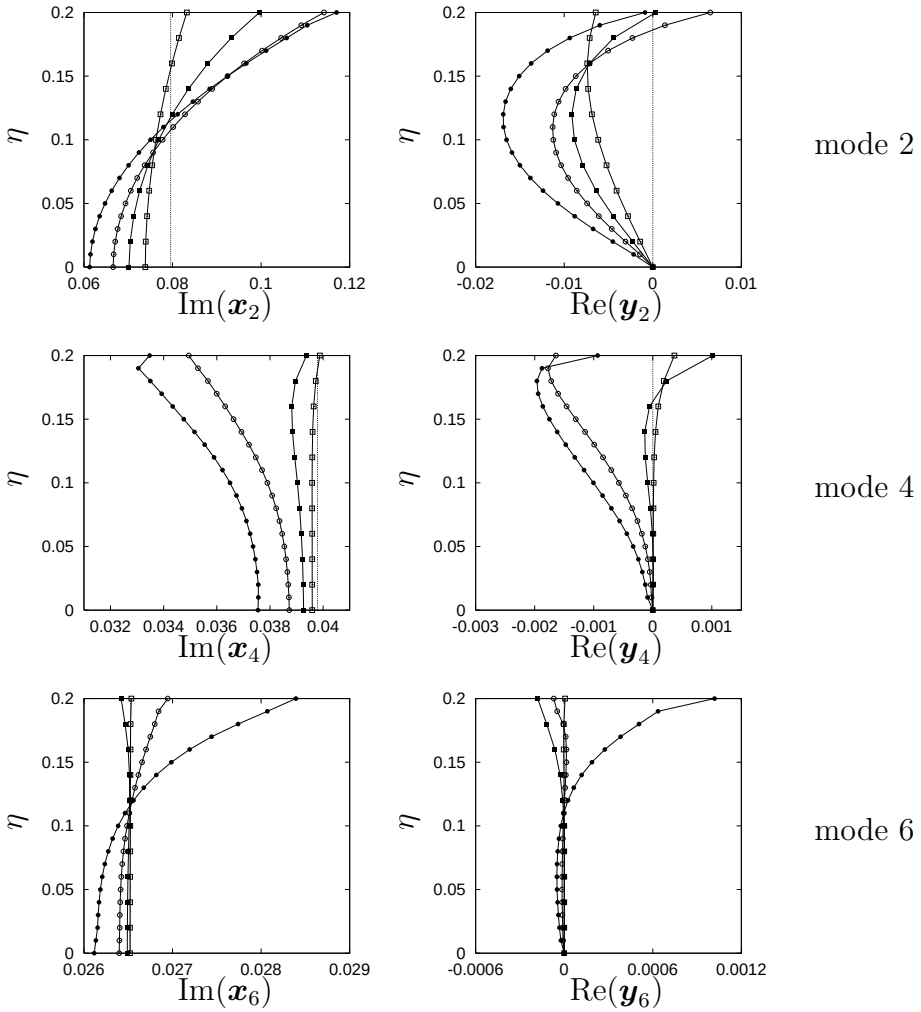

Figure 3: For the flow in Fig. 2, imaginary and real parts of Fourier's coefficients $\boldsymbol{x}_2$, $\boldsymbol{y}_2$ (first row), $\boldsymbol{x}_4$, $\boldsymbol{y}_4$ (second row) and $\boldsymbol{x}_6$, $\boldsymbol{y}_6$ (third row) are drawn vs. η, at times $t = T_2/4$ (squares), $T_2/2$ (filled squares), $3T_2/4$ (circles) and T_2 (filled circles). The corresponding values for the initial grid are drawn with dotted lines.

in which $\boldsymbol{x}^{(k)} = x^{(k)} + \mathrm{i}\, y^{(k)}$ is assumed of the order of the unity, for any k. In particular, $x^{(k)}$ and $y^{(k)}$ satisfy also the conditions $x^{(k)}(\pm l/2, \eta; t) \equiv 0$ and $y^{(k)}(\xi, 0; t) \equiv 0$: the first one is needed to enforce the bound $-l/2 \leq x < l/2$, while the second condition accounts for the presence of the bottom wall. The expansion (11) is inserted into Jacobi's determinant constraint (4), leading to the following relations:

$$\begin{aligned} x_\xi^{(1)} + y_\eta^{(1)} &= 0 \\ x_\xi^{(2)} + y_\eta^{(2)} &= -(x_\xi^{(1)} y_\eta^{(1)} - x_\eta^{(1)} y_\xi^{(1)}) \end{aligned} \tag{12}$$

at first and second order. Finally, all the perturbation fields are taken as periodic function of ξ, with period l.

Aim of the perturbation expansion lies in reducing the lagrangian pressure equation in the problem (7), in which $\mathcal{L}$ has variable coefficients, to a hierarchy of Poisson's problems. As a matter of fact, if the metrical coefficients (6) are expanded in power series of ε:

$$\begin{aligned} N^2 &= 1 + \varepsilon \underbrace{2 y_\eta^{(1)}}_{\nu^{(1)}} + \varepsilon^2 \underbrace{(2 y_\eta^{(2)} + {x_\eta^{(1)}}^2 + {y_\eta^{(1)}}^2)}_{\nu^{(2)}} + \dots \\ S &= 0 + \varepsilon \underbrace{(x_\eta^{(1)} + y_\xi^{(1)})}_{\sigma^{(1)}} + \varepsilon^2 \underbrace{(x_\eta^{(2)} + y_\xi^{(2)} + x_\xi^{(1)} x_\eta^{(1)} + y_\xi^{(1)} y_\eta^{(1)})}_{\sigma^{(2)}} + \dots \\ M^2 &= 1 + \varepsilon \underbrace{2 x_\xi^{(1)}}_{\mu^{(1)}} + \varepsilon^2 \underbrace{(2 x_\xi^{(2)} + {x_\xi^{(1)}}^2 + {y_\xi^{(1)}}^2)}_{\mu^{(2)}} + \dots \\ Q &= 0 + \varepsilon \underbrace{(-x_{\eta\eta}^{(1)} + y_{\xi\eta}^{(1)})}_{\chi^{(1)}} + \\ &\quad + \varepsilon^2 \underbrace{(-x_{\eta\eta}^{(2)} + y_{\xi\eta}^{(2)} + x_\eta^{(1)} x_{\xi\eta}^{(1)} + y_\eta^{(1)} y_{\xi\eta}^{(1)} - x_\xi^{(1)} x_{\eta\eta}^{(1)} - y_\xi^{(1)} y_{\eta\eta}^{(1)})}_{\chi^{(2)}} + \dots \\ R &= 0 + \varepsilon \underbrace{(x_{\xi\eta}^{(1)} - y_{\xi\xi}^{(1)})}_{\rho^{(1)}} + \\ &\quad + \varepsilon^2 \underbrace{(x_{\xi\eta}^{(2)} - y_{\xi\xi}^{(2)} + x_\xi^{(1)} x_{\xi\eta}^{(1)} + y_\xi^{(1)} y_{\xi\eta}^{(1)} - x_\eta^{(1)} x_{\xi\xi}^{(1)} - y_\eta^{(1)} y_{\xi\xi}^{(1)})}_{\rho^{(2)}} + \dots \end{aligned}$$

the 0-th order terms in the coefficients S, Q and R vanish, while the ones in M^2 and N^2 are unitary, leading to the power series expansion of $\mathcal{L}$:

$$\mathcal{L} = \nabla_{\boldsymbol{\xi}}^2 + \varepsilon \mathcal{L}^{(1)} + \varepsilon^2 \mathcal{L}^{(2)} + \dots \tag{13}$$

in which the differential operators $\mathcal{L}^{(k)}$ for $k \geq 1$ are given by:

$$\mathcal{L}^{(k)} = \nu^{(k)} \partial_{\xi\xi}^2 - 2\sigma^{(k)} \partial_{\xi\eta}^2 + \mu^{(k)} \partial_{\eta\eta}^2 + \chi^{(k)} \partial_\xi + \rho^{(k)} \partial_\eta \,.$$

The expansions (13) and $P = P^{(0)} + \varepsilon\, P^{(1)} + \varepsilon^2\, P^{(2)} + \ldots$ lead to the hierarchy of equations:

$$\begin{aligned} \nabla_{\boldsymbol{\xi}} P^{(0)} &= 0 \\ \nabla_{\boldsymbol{\xi}} P^{(1)} &= -\mathcal{L}^{(1)} P^{(0)} \\ \nabla_{\boldsymbol{\xi}} P^{(2)} &= -\mathcal{L}^{(1)} P^{(1)} - \mathcal{L}^{(2)} P^{(0)} + 2(u_\xi^{(1)} v_\eta^{(1)} - u_\eta^{(1)} v_\xi^{(1)}) \end{aligned}$$

at zero, first and second order. Differential problems for the pressure perturbations are obtained by expanding the boundary conditions on the pressure field. On the free surface ($\eta = h$) $P^{(k)} = g y^{(k)}$ holds for any k, while on the bottom wall ($\eta = 0$) the following relations are obtained:

$$\begin{aligned} P_\eta^{(0)} &= 0 \\ P_\eta^{(1)} &= 0 \\ P_\eta^{(2)} &= x_\eta^{(1)}\, P_\xi^{(1)} \end{aligned}$$

at zero, first and second order.

A corresponding hierarchy of dynamical equations may be written by inserting McLaurin's expansions for the flow (11) and for the pressure into the second equation of the system (7). At the zero order $P^{(0)} \equiv gh$, or $p^{(0)} = g\,(h - \eta)$, follows, while the hierarchy of dynamical equations:

$$\begin{aligned} x_{tt}^{(1)} &= -P_\xi^{(1)} \\ y_{tt}^{(1)} &= -P_\eta^{(1)} \\ x_{tt}^{(2)} &= y_\xi^{(1)}\, P_\eta^{(1)} - y_\eta^{(1)}\, P_\xi^{(1)} - P_\xi^{(2)} \\ y_{tt}^{(2)} &= x_\eta^{(1)}\, P_\xi^{(1)} - x_\xi^{(1)}\, P_\eta^{(1)} - P_\eta^{(2)} \end{aligned} \tag{14}$$

is deduced at first and second order.

Due to the assumed periodicity in ξ, the flow perturbations $x^{(k)}$ and $y^{(k)}$, as well as $P^{(k)}$, and the real (U) and imaginary (V) parts of the initial velocity field $\boldsymbol{U} = U + \mathrm{i}V$, are represented in terms of Fourier's series. For example:

$$x^{(k)}(\xi, \eta; t) = \sum_{m=-\infty}^{+\infty} \boldsymbol{x}_m^{(k)}(\eta; t)\, e^{\mathrm{i}\,\mathrm{M}\xi} \tag{15}$$

(hereafter, if the extremes of the series are not indicated, they are $-\infty$ and $+\infty$, respectively). In equation (12), $\boldsymbol{x}_m^{(k)}$ is a complex Fourier's coefficient, such that $\boldsymbol{x}_{-m}^{(k)} = \overline{\boldsymbol{x}}_m^{(k)}$, where overbar means complex conjugate. The m-th Fourier's coefficients for $y^{(k)}$, $P^{(k)}$, U and V are $\boldsymbol{y}_m^{(k)}$, $\boldsymbol{P}_m^{(k)}$, $\boldsymbol{U}_m$ and $\boldsymbol{V}_m$, respectively. In particular, from the incompressibility constraint, $\mathrm{i}\,\mathrm{M}\boldsymbol{U}_m + \boldsymbol{V}_{m,\eta} = 0$ follows.

At the 0-th order, Fourier's coefficients of the flow are given by:

$$\boldsymbol{x}_m^{(0)}(\eta; t) \equiv \begin{cases} 0 & \text{for } m = 0 \\ \mathrm{i}(-1)^m/\mathrm{M} & \text{for } m \neq 0, \end{cases} \qquad \boldsymbol{y}_m^{(0)}(\eta; t) \equiv \begin{cases} \eta & \text{for } m = 0 \\ 0 & \text{for } m \neq 0. \end{cases}$$

4.1 First order solution

The first order condition on Jacobi's determinant (12) leads to the useful relations among Fourier's coefficients of the perturbations (15):

$$\mathrm{i}\,\mathrm{M}\,\boldsymbol{x}_m^{(1)} + \boldsymbol{y}_{m,\eta}^{(1)} = 0\,,$$

from which it is easily shown that $\boldsymbol{y}_0^{(1)}(\eta;t) \equiv 0$. Also the corresponding Fourier's component $\boldsymbol{x}_0^{(1)}(\eta;t)$ vanishes, as it can be easily proved from the first order equation (14), by accounting for the assumed property of U, which has a zero mean value in ξ.

The first order m-th Fourier's component of the pressure P is obtained by solving the following problem:

$$\begin{cases} \boldsymbol{P}_{m,\eta\eta}^{(1)} - \mathrm{M}^2\boldsymbol{P}_m^{(1)} = 0 \\ \boldsymbol{P}_{m,\eta}^{(1)} = 0 \quad \text{for } \eta = 0, \quad \boldsymbol{P}_m^{(1)} = g\boldsymbol{y}_m^{(1)} \quad \text{for } \eta = h, \end{cases}$$

as:

$$\boldsymbol{P}_m^{(1)}(\eta;t) = g\,\frac{\cosh \mathrm{M}\eta}{\cosh \mathrm{M}h}\,\boldsymbol{y}_m^{(1)}(h;t)\,.$$

By inserting the above pressure in the dynamical equation (14) for $y^{(1)}$, it follows:

$$\ddot{\boldsymbol{y}}_m^{(1)} = -g\mathrm{M}\,\frac{\sinh \mathrm{M}\eta}{\cosh \mathrm{M}h}\,\boldsymbol{y}_m^{(1)}(h;t)\,,$$

which, by introducing the frequency and the corresponding period:

$$\nu_m = \sqrt{g\mathrm{M}\tanh \mathrm{M}h}\,, \quad T_m = \frac{2\pi}{\nu_m}\,, \tag{16}$$

see equation (13.25) in [7], leads to the following problem for the m-th Fourier's component of the free surface displacement $y^{(1)}(h;t)$:

$$\begin{cases} \ddot{\boldsymbol{y}}_m^{(1)}(h;t) + \nu_m^2\boldsymbol{y}_m^{(1)}(h;t) = 0 \\ \boldsymbol{y}_m^{(1)}(h;0) = 0\,, \quad \dot{\boldsymbol{y}}_m^{(1)}(h;0) = \boldsymbol{V}_m(h)\,. \end{cases}$$

By solving the above problem, the m-th Fourier's coefficient for $y^{(1)}(h;t)$ follows:

$$\boldsymbol{y}_m^{(1)}(h;t) = \frac{\boldsymbol{V}_m(h)}{\nu_m}\,\sin \nu_m t\,, \tag{17}$$

and also the corresponding Fourier's coefficient for the pressure:

$$\boldsymbol{P}_m^{(1)}(\eta;t) = g\,\frac{\cosh \mathrm{M}\eta}{\cosh \mathrm{M}h}\,\frac{\boldsymbol{V}_m(h)}{\nu_m}\,\sin \nu_m t\,. \tag{18}$$

Equation (17) gives the first order correction to the straight 0-th order elevation of the free surface ($y^{(0)}(h;t) \equiv h$). By looking at this correction,

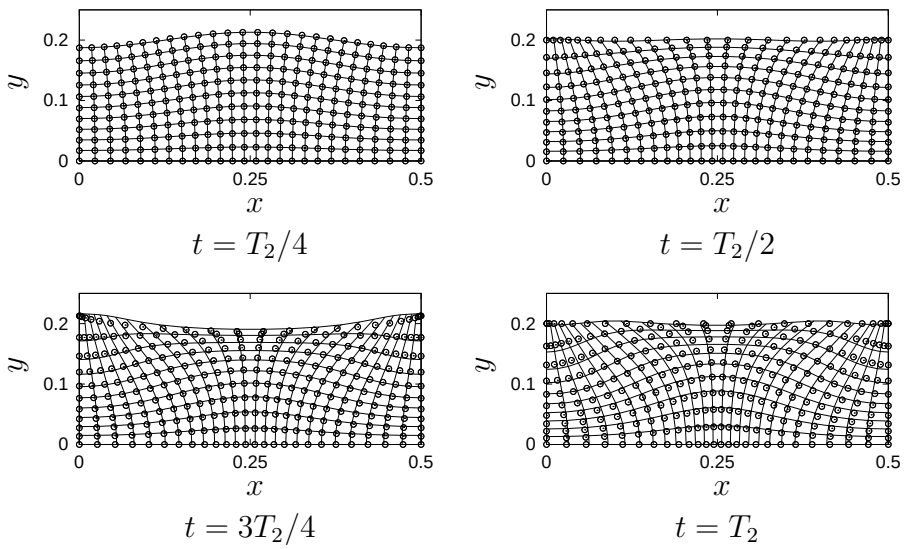

Figure 4: For the flow in Fig. 2, the computational grid (solid line) and the first order positions (symbols) are drawn at four times during the first period T_2. One grid point every two is represented, for the reader convenience. The free surface results flat at times $T_2/2$ and T_2 in the first order analytical solution.

several interesting observations can be made. A first important feature is that Fourier's components of the displacements have the same wavenumber of the initial velocity field, say α. This is due to the linear nature of such a solution. Secondly, for nonvanshing g the free surface elevation at the first order is periodical in time, with period T_m (16). This period is a decreasing function of g, *i.e.* the motion becomes slower and slower for decreasing g. As a matter of fact, in the limit for $g \to 0$, the first order solution (17) goes to $\boldsymbol{V}_m(h)\,t$, *i.e.* it is not more a periodical function of time. In the same limit, the pressure correction (18) vanishes, also. Thirdly, the wave amplitude depends on the ratio $\boldsymbol{V}_m(h)/\nu_m$: it is proportional to T_m and depends on the initial velocity along the free surface. It implies, for example, that an initial velocity, which vanishes at the free surface, has only second order corrections to the straight 0-th order shape, see Fig. 8 below.

The above results (17, 18) allows us to solve the problems for $\boldsymbol{x}_m^{(1)}$ and $\boldsymbol{y}_m^{(1)}$

(for $\eta < h$):

$$\begin{cases} \ddot{\boldsymbol{x}}_m^{(1)} = -\mathrm{i}\, g\, \mathrm{M}\, \dfrac{\cosh \mathrm{M}\eta}{\cosh \mathrm{M}h}\, \boldsymbol{V}_m(h)\, \dfrac{\sin \nu_m t}{\nu_m} \\ \boldsymbol{x}_m^{(1)}(\eta;0) \equiv 0\ , \ \ \dot{\boldsymbol{x}}_m^{(1)}(\eta;0) = \boldsymbol{U}_m(\eta) \end{cases}$$

$$\begin{cases} \ddot{\boldsymbol{y}}_m^{(1)} = -g\, \mathrm{M}\, \dfrac{\sinh \mathrm{M}\eta}{\cosh \mathrm{M}h}\, \boldsymbol{V}_m(h)\, \dfrac{\sin \nu_m t}{\nu_m} \\ \boldsymbol{y}_m^{(1)}(\eta;0) = 0\ , \ \ \dot{\boldsymbol{y}}_m^{(1)}(\eta;0) = \boldsymbol{V}_m(\eta)\ . \end{cases}$$

To this aim, the function of time:

$$F_m(t) = \frac{\sin \nu_m t}{\nu_m} - t\ , \tag{19}$$

which depends only on the modulus of the wavenumber $|\mathrm{M}|$, is introduced. About the function (19), it is worth noticing also that $F_m \to 0$ for $g \to 0$ and that $F_m(t) \sim -(\nu_m t)^2 t$ for small times t. The first order solution is written as:

$$\begin{aligned} x^{(1)} &= U\, t + \mathrm{i} \sum \frac{\cosh \mathrm{M}\eta}{\sinh \mathrm{M}h}\, \boldsymbol{V}_m(h)\, F_m\, e^{\mathrm{i}\, \mathrm{M}\xi} \\ y^{(1)} &= V\, t + \sum \frac{\sinh \mathrm{M}\eta}{\sinh \mathrm{M}h}\, \boldsymbol{V}_m(h)\, F_m\, e^{\mathrm{i}\, \mathrm{M}\xi} \\ P^{(1)} &= g \sum \frac{\cosh \mathrm{M}\eta}{\cosh \mathrm{M}h}\, \boldsymbol{V}_m(h)\, \frac{\sin \nu_m t}{\nu_m}\, e^{\mathrm{i}\, \mathrm{M}\xi} \end{aligned} \tag{20}$$

(for the sake of shortness, dependences on ξ, η and t are omitted). Note that $\nabla^2 x^{(1)} = \nabla^2 U\, t$ and $\nabla^2 y^{(1)} = \nabla^2 V\, t$ and that, for $g \to 0$, $\boldsymbol{x}^{(1)} \to \boldsymbol{U}\, t$. About the first order corrections (20) to the 0-order positions $\boldsymbol{x}^{(0)}(\boldsymbol{\xi};t) \equiv \boldsymbol{\xi}$, it is worth observing that they are not periodic in time, despite the periodic free surface elevation (17). This lack of periodicity is due to secular terms, proportional to the time t, which appear in the solution. Due to the assumed inviscid nature of the fluid, $x^{(1)}(\xi,0;t)$ results, in general, nonvanishing. Moreover, the term in Fourier's series for $x^{(1)}$ is odd in m, while the corresponding one for $y^{(1)}$ is even. So that, if $V(\xi,h) \propto \cos \mathrm{M}\xi$ (as will be the case, see below), $x^{(1)}$ behaves like $\sin \mathrm{M}\xi$ and $y^{(1)}$ like $\cos \mathrm{M}\xi$. In particular, $x^{(1)}$ is odd, while $y^{(1)}$ remains even.

A sample of first order solution is shown in Fig. 4, for the same flow of Section 3. The agreement between numerical solution and first order analytical one is satisfactory, unless a neighbourhood of the free surface at times $3T_2/4$ and T_2. A better approximation will be obtained at the second order, see Fig. 5 below.

4.2 Second order solution

The second order solution is deduced, following the same lines. First of all, it is worth noticing that the condition on the Jacobi determinant (11), at the

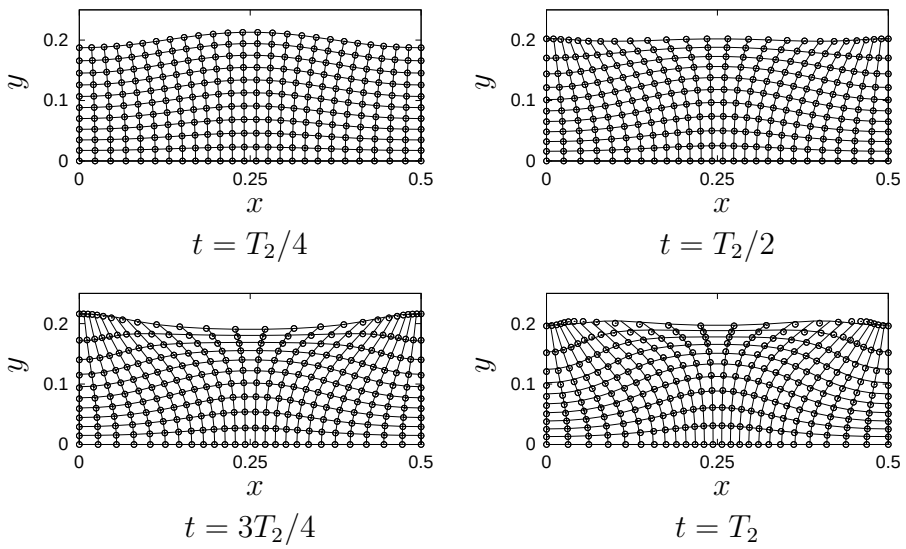

Figure 5: As in Fig. 4, but for the second order analytical solution.

second order, leads to the following relation:

$$\mathrm{i}\mathrm{M}\boldsymbol{x}_m^{(2)} + \boldsymbol{y}_m^{(2)} = -\mathrm{i} \sum_{r+q=m} \mathrm{R}\left(\boldsymbol{x}_r^{(1)}\boldsymbol{y}_{q,\eta}^{(1)} + \boldsymbol{x}_{r,\eta}^{(1)}\boldsymbol{y}_q^{(1)}\right),$$

from which Fourier's coefficient $\boldsymbol{y}_0^{(2)}$ follows:

$$\begin{aligned}\boldsymbol{y}_0^{(2)}(\eta;t) \;=\; -\mathrm{i} \sum_{r+q=0} \mathrm{R}\Big[\; & \boldsymbol{U}_r\boldsymbol{V}_q t^2 + \\ & + \frac{\boldsymbol{U}_r\boldsymbol{V}_q(h)\sinh \mathrm{R}\eta + \mathrm{i}\boldsymbol{V}_r(h)\boldsymbol{V}_q \cosh \mathrm{R}\eta}{\sinh \mathrm{R}h}\, tF_r + \\ & + \mathrm{i}\,\frac{\boldsymbol{V}_r(h)\boldsymbol{V}_q(h)}{2\sinh^2 \mathrm{R}h}\,\sinh 2\mathrm{R}\eta\, F_r^2\Big]\,.\end{aligned}$$

The m-th Fourier's component of the pressure perturbation $P^{(2)}$ satisfies the following differential problem:

$$\begin{cases} \boldsymbol{P}_{m,\eta\eta}^{(2)} - \mathrm{M}^2\boldsymbol{P}_m^{(2)} = \displaystyle\sum_{r+q=m} \Pi_{rq} \\ \boldsymbol{P}_{m,\eta}^{(2)} = \mathrm{i}\displaystyle\sum_{r+q=m} \mathrm{Q}\,\boldsymbol{x}_{r,\eta}^{(1)}\,\boldsymbol{P}_q^{(1)} \quad \text{for } \eta = 0 \\ \boldsymbol{P}_m^{(2)} = g\boldsymbol{y}_m^{(2)} \quad \text{for } \eta = h, \end{cases} \tag{21}$$

where Π_{rq} is the $r+p$-th Fourier's coefficient related to the sum of the quadratic terms $-\mathcal{L}^{(1)}P^{(1)}$ (first two rows) and $2(u_\xi^{(1)}v_\eta^{(1)} - u_\eta^{(1)}v_\xi^{(1)})$ (third row), while

$\mathcal{L}^{(2)}P^{(0)} \equiv 0$:

$$\begin{aligned}
\Pi_{rq} &= \mathrm{i}\mathrm{Q}[-2\mathrm{R}\mathrm{Q}\boldsymbol{x}_r^{(1)} + (\boldsymbol{U}_{r,\eta\eta} - \mathrm{R}^2\boldsymbol{U}_r)t]\boldsymbol{P}_q^{(1)} + \\
&\quad +[2\mathrm{i}\mathrm{Q}(\boldsymbol{x}_{r,\eta}^{(1)} + \mathrm{i}\mathrm{R}\boldsymbol{y}_r^{(1)}) + (\boldsymbol{V}_{r,\eta\eta} - \mathrm{R}^2\boldsymbol{V}_r)t]\boldsymbol{P}_{q,\eta}^{(1)} + 2\boldsymbol{y}_{r,\eta}^{(1)}\boldsymbol{P}_{q,\eta\eta}^{(1)} + \\
&\quad +2\mathrm{i}(\mathrm{R}\dot{\boldsymbol{x}}_r^{(1)}\dot{\boldsymbol{y}}_{q,\eta}^{(1)} - \mathrm{Q}\dot{\boldsymbol{x}}_{r,\eta}^{(1)}\dot{\boldsymbol{y}}_q^{(1)}) \\
&= \frac{g\mathrm{Q}}{\cosh \mathrm{Q}h}\,\boldsymbol{V}_q(h)\,\frac{\sin\nu_q t}{\nu_q}\,\left\{\frac{4\mathrm{R}\mathrm{Q}}{\sinh \mathrm{R}h}\,\boldsymbol{V}_r(h)\,F_r\cosh(\mathrm{R}-\mathrm{Q})\eta + \right. \\
&\quad + \left[\ \mathrm{i}\,(\boldsymbol{U}_{r,\eta\eta}\cosh \mathrm{Q}\eta + 2\mathrm{Q}\boldsymbol{U}_{r,\eta}\sinh \mathrm{Q}\eta - \mathrm{R}(\mathrm{R}+2\mathrm{Q})\boldsymbol{U}_r\cosh \mathrm{Q}\eta) + \right. \\
&\quad \left. \left. +(\boldsymbol{V}_{r,\eta\eta}\sinh \mathrm{Q}\eta + 2\mathrm{Q}\boldsymbol{V}_{r,\eta}\cosh \mathrm{Q}\eta - \mathrm{R}(\mathrm{R}+2\mathrm{Q})\boldsymbol{V}_r\sinh \mathrm{Q}\eta)\ \right]\ t\ \right\} + \\
&\quad +2\mathrm{i}\ \left[\mathrm{R}\boldsymbol{U}_r\boldsymbol{V}_{q,\eta} - \mathrm{Q}\boldsymbol{U}_{r,\eta}\boldsymbol{V}_q + \right. \\
&\quad +\mathrm{i}\mathrm{R}\,\frac{\cosh \mathrm{R}\eta}{\sinh \mathrm{R}h}\,\boldsymbol{V}_r(h)\,\boldsymbol{V}_{q,\eta}\,\dot{F}_r - \mathrm{Q}\,\frac{\sinh \mathrm{Q}\eta}{\sinh \mathrm{Q}h}\,\boldsymbol{V}_q(h)\boldsymbol{U}_{r,\eta}\,\dot{F}_q + \\
&\quad +\mathrm{R}\mathrm{Q}\,\frac{\cosh \mathrm{Q}\eta}{\sinh \mathrm{Q}h}\,\boldsymbol{V}_q(h)\,\boldsymbol{U}_r\,\dot{F}_q - \mathrm{i}\mathrm{R}\mathrm{Q}\,\frac{\sinh \mathrm{R}\eta}{\sinh \mathrm{R}h}\,\boldsymbol{V}_r(h)\boldsymbol{V}_q\,\dot{F}_r + \\
&\quad \left. +\mathrm{i}\mathrm{R}\mathrm{Q}\,\frac{\cosh(\mathrm{R}-\mathrm{Q})\eta}{\sinh \mathrm{R}h\sinh \mathrm{Q}h}\,\boldsymbol{V}_r(h)\boldsymbol{V}_q(h)\,\dot{F}_r\dot{F}_q\ \right]\ ,
\end{aligned}$$

In the solution of the differential problem (21), the following integral of Π_{rq} will be used:

$$\begin{aligned}
&\boldsymbol{C}_{rq,m}(\eta) = \int_0^\eta d\zeta\ \Pi_{rq}(\zeta;t)\ \cosh \mathrm{M}\zeta \\
&= \quad \boldsymbol{C}_{rq,m}^{(1)}(\eta) + \boldsymbol{C}_{rq,m}^{(2)}(\eta)\,t\sin\nu_q t + \\
&\quad +\boldsymbol{C}_{rq,m}^{(3)}(\eta)\ \sin\nu_r t\sin\nu_q t + \boldsymbol{C}_{rq,m}^{(4)}(\eta)\,(1-\cos\nu_r t) + \\
&\quad +\boldsymbol{C}_{rq,m}^{(5)}(\eta)\,(1-\cos\nu_q t) + \boldsymbol{C}_{rq,m}^{(6)}(\eta)\,(1-\cos\nu_r t)(1-\cos\nu_q t)
\end{aligned} \tag{22}$$

(note that $1-\cos\nu_r t$ vanishes for $g \to 0$), as well as the one ($\boldsymbol{S}_{rq,m}$) with $\sinh \mathrm{M}\zeta$ replacing $\cosh \mathrm{M}\zeta$. They are listed in Appendix B, in terms of the following integrals of the initial velocity field:

$$\begin{aligned}
\boldsymbol{c}_{r,k}^{u}(\eta) &= \int_0^\eta d\zeta\,\boldsymbol{U}_r(\zeta)\ \cosh \mathrm{K}\zeta \\
\boldsymbol{c}_{rq,k}^{uu}(\eta) &= \int_0^\eta d\zeta\,\boldsymbol{U}_r(\zeta)\,\boldsymbol{U}_q(\zeta)\ \cosh \mathrm{K}\zeta \\
\boldsymbol{c}_{rq,k}^{uv}(\eta) &= \int_0^\eta d\zeta\,\boldsymbol{U}_r(\zeta)\,\boldsymbol{V}_q(\zeta)\ \cosh \mathrm{K}\zeta
\end{aligned} \tag{23}$$

and the analogous ones ($\boldsymbol{s}_{r,k}^{u}$, $\boldsymbol{s}_{rq,k}^{uu}$ and $\boldsymbol{s}_{rq,k}^{uv}$) with $\sinh \mathrm{K}\zeta$ replacing $\cosh \mathrm{K}\zeta$. The integrals $\boldsymbol{c}_{\alpha,k}^{u}$, $\boldsymbol{c}_{\alpha\alpha,k}^{uu}$, $\boldsymbol{c}_{\alpha\alpha,k}^{uv}$ and the analogous ones with $\sinh \mathrm{K}\zeta$ for the initial velocities (8) are also listed in Appendix B.

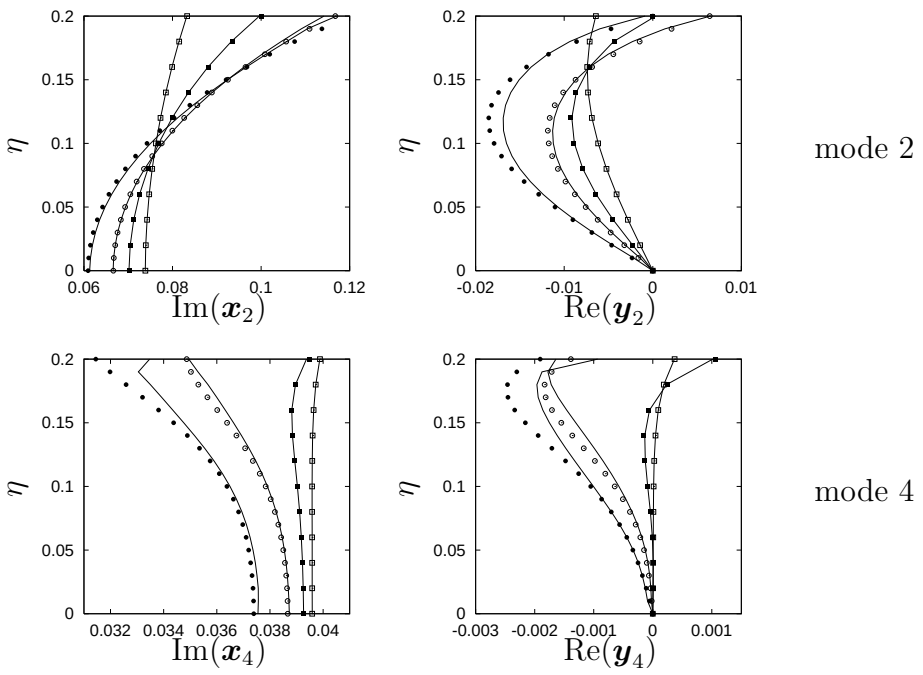

Figure 6: For the flow in Fig. 2, imaginary and real parts of Fourier's coefficients $\boldsymbol{x}_2$, $\boldsymbol{y}_2$ (first row), $\boldsymbol{x}_4$, $\boldsymbol{y}_4$ (second row) are drawn vs. η. Second order analytical solutions are indicated with boxes ($t = T_2/4$), filled boxes ($T_2/2$), circles ($3T_2/4$) and filled circles (T_2). The solid curves represent the corresponding quantities shown above (see Fig. 3), from the numerical simulation.

The m-th Fourier's component of the pressure $P^{(2)}$ is then given by:

$$\begin{aligned}
\boldsymbol{P}_m^{(2)} &= g\,\frac{\cosh \mathrm{M}\eta}{\cosh \mathrm{M}h}\,\boldsymbol{y}_m^{(2)}(h;t) + \\
&\quad -\frac{\mathrm{i}}{\mathrm{M}}\,\frac{\sinh \mathrm{M}(h-\eta)}{\cosh \mathrm{M}h}\sum_{r+q=m}\nu_q\,\frac{\boldsymbol{U}_{r,\eta}(0)\boldsymbol{V}_q(h)}{\sinh \mathrm{Q}h}\;\; t\sin\nu_q t + \\
&\quad +\frac{1}{\mathrm{M}}\sum_{r+q=m}\int_0^\eta d\zeta\;\sinh \mathrm{M}(\eta-\zeta)\Pi_{rq}(\zeta;t) + \\
&\quad -\frac{1}{\mathrm{M}}\,\frac{\cosh \mathrm{M}\eta}{\cosh \mathrm{M}h}\sum_{r+q=m}\int_0^h d\zeta\;\sinh \mathrm{M}(h-\zeta)\Pi_{rq}(\zeta;t) \qquad (24)
\end{aligned}$$

and, by inserting the above Fourier's component of the pressure in the dynamical equation (14) for $y^{(2)}$, it follows:

$$\ddot{\boldsymbol{y}}_m^{(2)} = -\nu_m^2\,\frac{\sinh \mathrm{M}\eta}{\sinh \mathrm{M}h}\,\boldsymbol{y}_m^{(2)}(h;t) +$$

$$
\begin{aligned}
&+\sum_{r+q=m}\Big[\,\tilde{\boldsymbol{C}}^{(2)}_{rq,m}(\eta)\,t\sin\nu_q t+\tilde{\boldsymbol{C}}^{(3)}_{rq,m}(\eta)\;\sin\nu_r t\sin\nu_q t\,\Big]\,i+\\
&+\frac{\sinh \mathrm{M}\eta}{\cosh \mathrm{M}h}\sum_{r+q=m}\int_0^h d\zeta\;\sinh \mathrm{M}(h-\zeta)\Pi_{rq}(\zeta;t)+\\
&-\sum_{r+q=m}\int_0^\eta d\zeta\;\cosh \mathrm{M}(\eta-\zeta)\Pi_{rq}(\zeta;t)\;,
\end{aligned}
\tag{25}
$$

in which the following positions are used:

$$
\begin{aligned}
\tilde{\boldsymbol{C}}^{(2)}_{rq,m}(\eta) &= \frac{\nu_q \boldsymbol{V}_q(h)}{\sinh \mathrm{Q}h}\Bigg[-\mathrm{i}\frac{\cosh \mathrm{M}(h-\eta)}{\cosh \mathrm{M}h}\,\boldsymbol{U}_{r,\eta}(0)+\\
&\qquad +\mathrm{i}\,(\boldsymbol{U}_{r,\eta}\;\cosh \mathrm{Q}\eta-\mathrm{R}\boldsymbol{U}_r\sinh \mathrm{Q}\eta)+\\
&\qquad +\mathrm{R}\,\frac{\sinh(\mathrm{R}-\mathrm{Q})\eta}{\sinh \mathrm{R}h}\,\boldsymbol{V}_r(h)\Bigg]\\
\tilde{\boldsymbol{C}}^{(3)}_{rq,m}(\eta) &= -\mathrm{R}\,\frac{\nu_q}{\nu_r}\,\frac{\sinh(\mathrm{R}-\mathrm{Q})\eta}{\sinh \mathrm{R}h\sinh \mathrm{Q}h}\,\boldsymbol{V}_r(h)\boldsymbol{V}_q(h)\;.
\end{aligned}
$$

This equation is written on the free surface ($\eta = h$), leading to the following problem on $\boldsymbol{y}_m(h;t)$:

$$
\begin{cases}
\ddot{\boldsymbol{y}}^{(2)}_m(h;t)+\nu_m^2\boldsymbol{y}^{(2)}_m(h;t)=\boldsymbol{T}(t)\\
\boldsymbol{y}^{(2)}_m(h;0)=0\;,\;\;\dot{\boldsymbol{y}}^{(2)}_m(h;0)=0\;.
\end{cases}
\tag{26}
$$

whose forcing term is given by the following relation:

$$
\begin{aligned}
\boldsymbol{T}(t) &= \sum_{r+q=m}\Big[\;\boldsymbol{T}^{(1)}_{rq,m}+\boldsymbol{T}^{(2)}_{rq,m}\,t\sin\nu_q t+\boldsymbol{T}^{(3)}_{rq,m}\;\sin\nu_r t\sin\nu_q t+\\
&\qquad +\boldsymbol{T}^{(4)}_{rq,m}(1-\cos\nu_r t)+\boldsymbol{T}^{(5)}_{rq,m}\,(1-\cos\nu_q t)+\\
&\qquad +\boldsymbol{T}^{(6)}_{rq,m}\,(1-\cos\nu_r t)(1-\cos\nu_q t)\,\Big]\;,
\end{aligned}
\tag{27}
$$

where the coefficients:

$$
\begin{aligned}
\boldsymbol{T}^{(1)}_{rq,m} &= -\frac{\boldsymbol{C}^{(1)}_{rq,m}(h)}{\cosh \mathrm{M}h} & \boldsymbol{T}^{(2)}_{rq,m} &= \tilde{\boldsymbol{C}}^{(2)}_{rq,m}(h)-\frac{\boldsymbol{C}^{(2)}_{rq,m}(h)}{\cosh \mathrm{M}h}\\
\boldsymbol{T}^{(3)}_{rq,m} &= \tilde{\boldsymbol{C}}^{(3)}_{rq,m}(h)-\frac{\boldsymbol{C}^{(3)}_{rq,m}(h)}{\cosh \mathrm{M}h} & \boldsymbol{T}^{(4)}_{rq,m} &= -\frac{\boldsymbol{C}^{(4)}_{rq,m}(h)}{\cosh \mathrm{M}h}\\
\boldsymbol{T}^{(5)}_{rq,m} &= -\frac{\boldsymbol{C}^{(5)}_{rq,m}(h)}{\cosh \mathrm{M}h} & \boldsymbol{T}^{(6)}_{rq,m} &= -\frac{\boldsymbol{C}^{(6)}_{rq,m}(h)}{\cosh \mathrm{M}h}
\end{aligned}
$$

have been used. The solution of such a problem is written, for $m \neq 0$, as:

$$
\begin{aligned}
\boldsymbol{y}^{(2)}_m(h;t) &= \frac{1}{\nu_m}\sum_{\substack{r+q=m\\ r,q\neq 0}}\Big[\;\boldsymbol{T}^{(1)}_{rq,m}\,\mathcal{I}^{(1)}_m(t)+\boldsymbol{T}^{(2)}_{rq,m}\,\mathcal{I}^{(2)}_{q,m}(t)+\\
&\qquad +\boldsymbol{T}^{(3)}_{rq,m}\,\mathcal{I}^{(3)}_{rq,m}(t)+\boldsymbol{T}^{(4)}_{rq,m}\,\mathcal{I}^{(4)}_{r,m}(t)+\\
&\qquad +\boldsymbol{T}^{(5)}_{rq,m}\,\mathcal{I}^{(4)}_{q,m}(t)+\boldsymbol{T}^{(6)}_{rq,m}\,\mathcal{I}^{(5)}_{rq,m}(t)\;\Big]\;.
\end{aligned}
\tag{28}
$$

The functions of time in equation (28) are evaluated in Appendix B. About these functions, it is worth noticing that $\mathcal{I}_m^{(1)}$, $\mathcal{I}_{rq,m}^{(3)}$, $\mathcal{I}_{r,m}^{(4)}$ and $\mathcal{I}_{rq,m}^{(5)}$ are periodic in time. More specifically, they are linear combinations of cosines at frequences ν_m, ν_r, ν_q, $\nu_r + \nu_q$ and $\nu_r - \nu_q$. On the contrary, the function $\mathcal{I}_{q,m}^{(2)}$ is not a periodic one. As a matter of fact, the secular term $t \sin \nu_q t$ appears in that function. For this reason, the second order elevation is not a periodic function of time.

By inserting Fourier's coefficient (28) for the free surface vertical displacement in the dynamical equation (25), it can be integrated starting from homogeneous conditions on velocity and position. The integrals in time, as the following one:

$$\int_0^t d\tau' \int_0^{\tau'} d\tau'' \, \mathcal{I}_m^{(1)}(\tau'') = \mathcal{J}_m^{(5)}(t) \, ,$$

are evaluated in Appendix B. Finally, the dynamical equation (14) for $x^{(2)}$ is written as:

$$\begin{aligned} \ddot{\boldsymbol{x}}_m^{(2)} \;=\; & \mathrm{i} \sum_{\substack{r+q=m \\ r,q \neq 0}} \frac{\nu_q \boldsymbol{V}_q(h)}{\sinh \mathrm{Q} h} \times \\ & \times \left\{ \mathrm{R} \sinh \mathrm{Q}\eta \left[\boldsymbol{V}_r t + \frac{\sinh \mathrm{R}\eta}{\sinh \mathrm{R} h} \boldsymbol{V}_r(h) F_r \right] + \right. \\ & \left. - \cosh \mathrm{Q}\eta \left[\boldsymbol{V}_{r,\eta} t + \mathrm{R} \, \frac{\cosh \mathrm{R}\eta}{\sinh \mathrm{R} h} \boldsymbol{V}_r(h) F_r \right] \right\} \sin \nu_q t - \mathrm{i}\mathrm{M} P_m^{(2)} \, , \end{aligned} \tag{29}$$

where Fourier's coefficient for the pressure $P_m^{(2)}$ is given by equation (24). The acceleration (29) is integrated in time, starting from homogeneous conditions on velocity and position. Results listed in Appendix B are also used.

A sample of second order solution is shown in Fig. 5, where the positions from the numerical simulation and the analytical solution are superimposed. Differences appear just at the final time (T_2), only in a small neighbourhood of the free surface. In a more quantitative way, the same picture may be deduced from Fig. 6, where analytical Fourier's coefficients:

$$\boldsymbol{x}_m = \boldsymbol{x}_m^{(0)} + \varepsilon \boldsymbol{x}_m^{(1)} + \varepsilon^2 \boldsymbol{x}_m^{(2)} + \ldots$$

(an analogous expansion is adopted for $\boldsymbol{y}_m$) and the numerical ones are drawn vs. η at the same times of Fig. 5. The agreement for the mode 2 is quite good, unless the last time. However, mode 4 appears to be affected by larger errors, for reasons that will be explained in the next section.

5 Discussion

The behaviour of the analytical solution vs. the numerical simulation is briefly investigated.

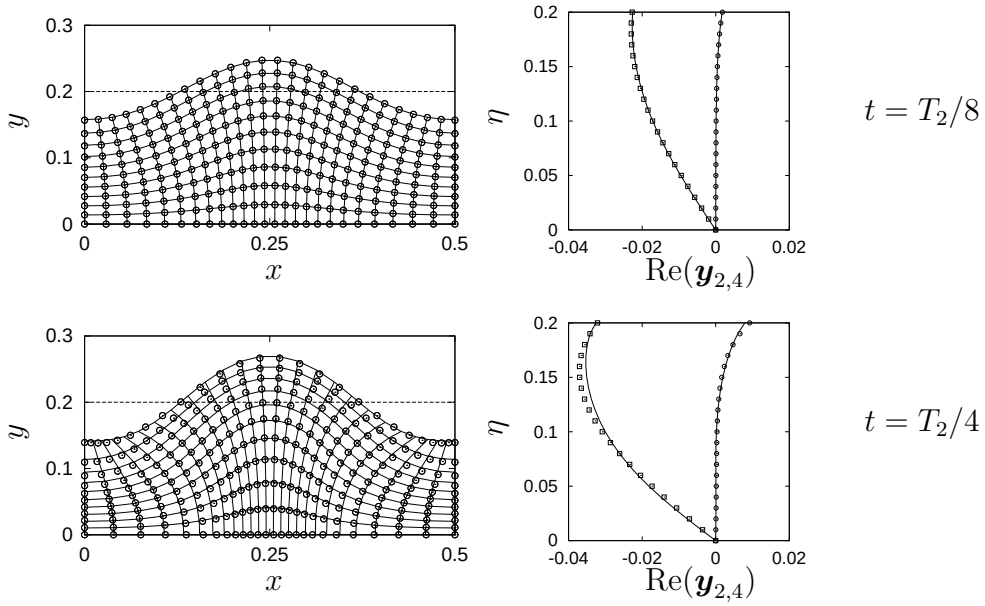

Figure 7: For the flow with $h = 0.2$, $\alpha = 2$, $\beta = 1$ and $\varepsilon = 0.1$ positions (one grid node every four, left column) and Fourier coefficients $\boldsymbol{y}_2$ and $\boldsymbol{y}_4$ vs. η (one symbol every two nodes, right column) are drawn at times $T_2/8$ and $T_2/4$. A computational grid 201×41 has been used, with a time step $\Delta t = T_2/3200 \simeq 7.884 \cdot 10^{-4}$. Results of the numerical simulation are drawn with solid lines, while the initial position of the free surface is drawn with a dashed line. About the second order solution, positions are drawn by circles, coefficients $\boldsymbol{y}_2$ with squares and $\boldsymbol{y}_4$ with circles. During the numerical integration, the error on the conservation of the area of the fluid domain grows up to reach $4.302 \cdot 10^{-4}$ at time $T_2/4$.

About the analytical solution just derived in Section 4, an introductive consideration appears to be important. The initial velocity field (8) has nonvanishing Fourier's coefficients at wavenumbers $\mathrm{A}_{\pm\alpha} = \pm 2\pi\alpha/l$, for a given integer α. As stated above, the first order solution (20) has nonvanishing Fourier's components at the same wavenumbers ($\mathrm{A}_{\pm\alpha}$), due to its linear nature. Moreover, the second order solution possesses nonvanishing Fourier's components at wavenumbers $\mathrm{A}_{2\alpha}$, 0 and $\mathrm{A}_{-2\alpha}$, which account for quadratic nonlinearities, only.

However, numerical simulation exhibits modes at any wavenumber M, even if their amplitudes decrease for $|\mathrm{M}| \to \infty$. They are produced by nonlinear interactions, starting from the two modes (A_α and $\mathrm{A}_{-\alpha}$, say) which have been directly excited by the initial condition. Modes at wavenumbers different from $\mathrm{A}_{\pm\alpha}$ take a certain time in order to become significant. This mechanism is

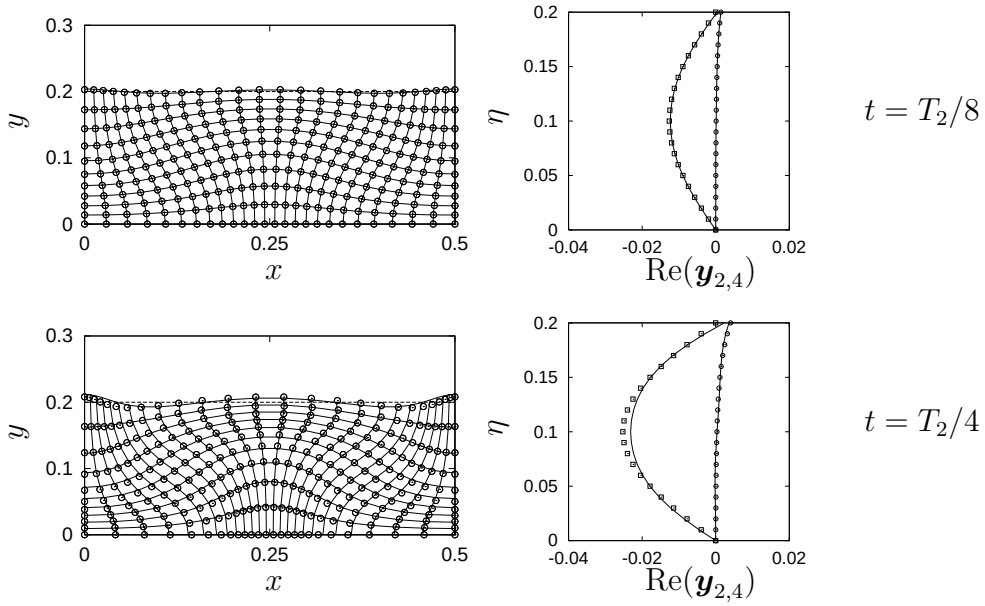

Figure 8: As in Fig. 7, but for $\beta = 2$. The maximum error on the conservation of the area of the fluid domain is $5.092 \cdot 10^{-4}$.

absent in the approximated analytical solution, so the agreement between the two solutions remains a satisfactory one for small times, only. In order to reach a excellent agreement, times t for which $\varepsilon\, t$ (*i.e.* the order of magnitude of the displacement of each fluid particle from its initial position) results $\ll 1$ may be considered, only.

Another important source of disagreement between analytical and numerical solutions lies in the errors induced by the space-time discretization of the system (7) adopted in the numerical simulations. In this framework, a very difficult matter is the analysis of the effects of the truncation errors on the pressure field, due to the presence of the metrical terms (6) in the (discrete) operator $\mathcal{L}$ (5). They are evaluated through bi-linear intepolation formulae at the present time, but this important issue is still under investigation. The same terms lead to nonlinearities in the evolution equation of Fourier's coefficients whose effects are unpredictable at the present time.

In Section 4 the analytical solutions at first (see Fig. 4) and second order (see Fig. 5) have been compared with the numerical solution discussed in Section 3.1 (see Fig. 2). A satisfactory agreement in terms of the lagrangian positions has been reached. A more quantitative comparison is possible by looking at Fourier's coefficients (see Fig. 6). In this flow, the perturbation parameter ε has been chosen quite small, in order to ensure a long-time agreement between the two solutions. Unfortunately, ε^3 and errors in the numerical solution (measured in terms of conservation of the fluid domain area) become

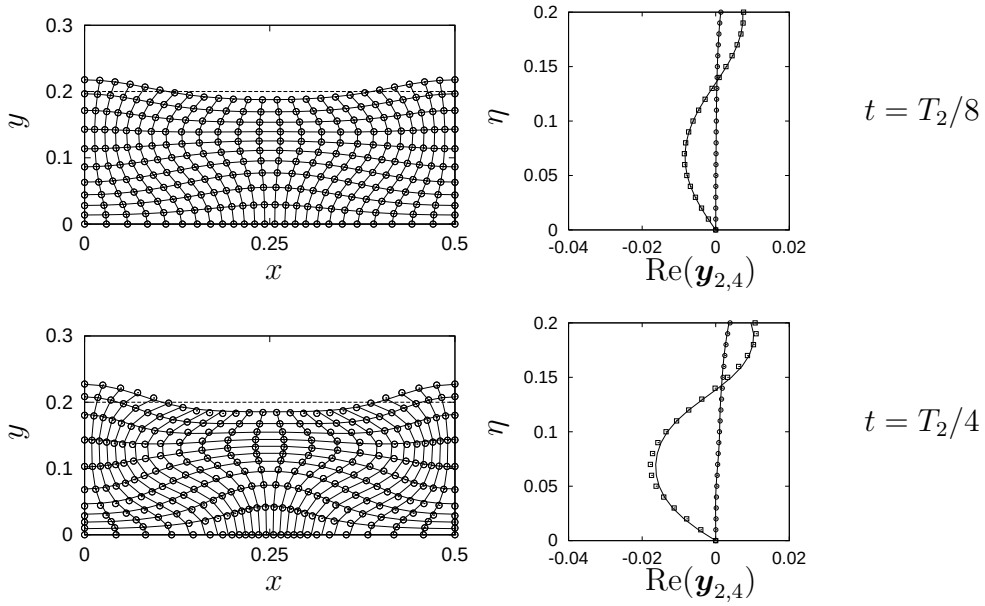

Figure 9: As in Fig. 7, but for $\beta = 3$. The maximum error on the conservation of the area of the fluid domain is $5.066 \cdot 10^{-4}$.

of the same order of magnitude in the time period under investigation. So, if the effects of the truncation of the power series (11) at terms of order ε^2 have to be investigated, a quite different strategy must be adopted. Smaller times and quite larger ε must be considered.

In Figg. 7, 8 and 9 the flow with $\varepsilon = 0.1$ is investigated, for three different initial conditions. The parameter α (*i.e.*, the wavenumbers $\mathrm{A}_{\pm\alpha}$ directly excited by the initial condition) is always fixed at 2 (so that the period remains T_2, as before), but the shape in η of the velocity field (8) is changed, by choosing $\beta = 1$ (Fig. 7), $\beta = 2$ (Fig. 8) and $\beta = 3$ (Fig. 9). Note that, β being at the denominator of ρ, the intensity of the vertical velocity V diminishes for growing β. Moreover, V vanishes on the free surface for $\beta = 2$.

For $\beta = 1$ the free surface elevation (difference between maximum and minimum height) reaches 65% of the initial depth h at $t = T_2/2$. Despite a so large deformation, the agreement between numerical and analytical solutions remains quite good, as it follows from Fourier's coefficients, also. Small differences appear just in a neighbourhood of the free surface. The flow with $\beta = 2$ is quite interesting, occurring with a nearly stationary free surface: the elevation reaches its maximum of about 9% of h at $t = T_2/2$. Note that the real part of Fourier coefficient $\boldsymbol{y}_2$ vanishes just below the free surface (at $\eta \simeq= 0.196$), while V is zero on that surface (at $\eta = h = 0.2$). Large deformations appear on the bottom wall, while the agreement between the solutions remains satisfactory. The flow with $\beta = 3$ exhibits large deformations below

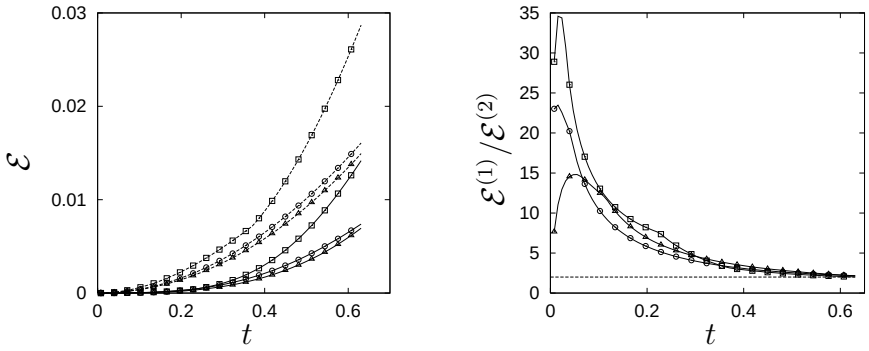

Figure 10: On the left, the errors $\mathcal{E}^{(1)}$ (dashed lines) and $\mathcal{E}^{(2)}$ (solid) are drawn vs. time, for $0 < t < T_2/4 \simeq 0.63078$, for the flows in Fig. 7 (squares), Fig. 8 (circles) and Fig. 9 (triangles). On the right, the corresponding ratios $\mathcal{E}^{(1)}/\mathcal{E}^{(2)}$ are drawn vs. time. The dashed line identifies the asymptotic value $\mathcal{E}^{(1)}/\mathcal{E}^{(2)} \equiv 2$.

the free surface, whose elevation reaches a maximum of 20% of h $t = T_2/2$. Here, the real part of Fourier coefficient $\boldsymbol{y}_2$ vanishes at $\eta \simeq= 0.138$, while V becomes zero at $\eta \simeq 0.133$. Even for this flow, the agreement between the two solutions appears quite good.

A more quantitative picture of the differences between the analytical and the numerical solution is obtained by considering the following norms:

$$\mathcal{E}^{(1)} = \|\boldsymbol{x} - [\boldsymbol{\xi} + \varepsilon \boldsymbol{x}^{(1)}]\|_\infty \,, \quad \mathcal{E}^{(2)} = \|\boldsymbol{x} - [\boldsymbol{\xi} + \varepsilon \boldsymbol{x}^{(1)} + \varepsilon^2 \boldsymbol{x}^{(2)}]\|_\infty \,,$$

i.e. the maximum distance between numerical ($\boldsymbol{x}$) and analytical positions at first ($\boldsymbol{\xi} + \varepsilon \boldsymbol{x}^{(1)}$) and second order ($\boldsymbol{\xi} + \varepsilon \boldsymbol{x}^{(1)} + \varepsilon^2 \boldsymbol{x}^{(2)}$), evaluated on the computational grid. These norms are drawn vs. time in Fig. 10, for the three sample cases discussed above. In the first flow ($\beta = 1$) the second order solution exhibits a distance from the numerical one quite relevant, at least for $T_2/8 < t < T_2/2$. As expected, in the other two cases the final values of $\mathcal{E}^{(1)}$ and $\mathcal{E}^{(2)}$ are of the order of magnitude of ε^2 and ε^3, respectively. On the right of Fig. 10, the ratio $\mathcal{E}^{(1)}/\mathcal{E}^{(2)}$ is also drawn vs. time. Note the excellent initial behaviour of the second order solution. At later times, the growth of modes which cannot be followed by the present analytical approach leads to larger $\mathcal{E}^{(2)}$, until $\mathcal{E}^{(2)}$ becomes about half $\mathcal{E}^{(1)}$ at times of the order of $T_2/4$.

6 Conclusions and Perspectives

A comparison between numerical simulations of a two-dimensional, free surface flow of an inviscid fluid and an analytical solution is performed. This latter

solution is obtained through a small perturbation expansion of the lagrangian equations of motion with respect to the amplitude ε of the initial velocity field. The analysis shows that an agreement between the two approaches is reached, at least for times t such that $\varepsilon t \ll 1$. At later times, modes which cannot be followed by the analytical solution become important, leading to a less satisfactory agreement. The numerical simulations are performed through a second order finite difference approach, with staggered pressure. The time integration is performed with a predictor-corrector Runge-Kutta second order scheme, in which the constraint of diverge-free velocity is explicitly enforced in the corrector substep. Here, a deeper understanding of the effects of the discretization errors appears to be necessary.

In the author intention, the present paper is the starting point in order to investigate a conformal mapping approach in lagrangian coordinates. The main idea lies in transforming the lagrangian coordinates $\boldsymbol{\xi} = \xi + \mathrm{i}\,\eta$ to new ones $\boldsymbol{\Xi} = \Xi + \mathrm{i}\,H$:

$$\begin{cases} x[\xi(\Xi, H), \eta(\Xi, H)] = X(\Xi, H) \\ y[\xi(\Xi, H), \eta(\Xi, H)] = Y(\Xi, H)\,, \end{cases}$$

such that the complex function $\boldsymbol{X}(\boldsymbol{\Xi})$ results an analytical one, *i.e.* Cauchy-Riemann's conditions:

$$X_\Xi = Y_H\,, \quad X_H = -Y_\Xi\,,$$

are satisfied. It can be shown that the new lagrangian coordinates verify the equations:

$$\mathcal{L}\,\Xi = 0\,, \quad \mathcal{L}\,H = 0\,, \tag{30}$$

where the second order differential operator $\mathcal{L}$ is the lagrangian form of the Laplace operator, still defined in equation (5). By solving equations (30) in the rectangular domain $[-l/2, l/2) \times [0, h]$ of the (ξ, η) plane, the physical domain is mapped, for example, in an annular region of the plane (Ξ, H). In this way the periodicity along ξ may be accounted for once for all and the mapping results to be a conformal one.

The above approach will be object of future work, together with a re-writing of the numerical algorithm presented in Section 3 at fourth order in space and time. Comparisons with numerical conformal mappings [1] will be also performed.

References

[1] B. Cheng Li and S. Syngellakis, Numerical conformal mapping based on the generalized conjugation operator, *Mathematics of Computation*, 67 (1998), 619 – 639.

[2] S.R. Idelsohn, E. Oñate and C. Sacco, Finite element solution of free-surface ship-wave problems, *Int. J. for Numerical Methods in Engineering*, 45 (1999), 503 – 528.

[3] M.S. Longuet-Higgins and E.D. Cokelet, The deformation of step surface waves on water, I. A numerical method of computation, *Proc. Royal Society London* A, 350 (1976), 1 – 26.

[4] A.S. Monin and M.A. Yaglom, Statistical Fluid Mechanics, vol. 1, MIT Press (1975).

[5] A.L. New, P. McIver and D.H. Peregrine, Computations of overturning waves, *J. Fluid Mechanics*, 150 (1985), 233 – 254.

[6] B.E. Protopopov, An efficient numerical method for calculation of strongly nonlinear water waves, *Computational Technologies*, 3 (1998), 55 – 71.

[7] G.B. Whitham, Linear and nonlinear waves, Wiley (1974).

[8] E.I. Yakubovich and D.A. Zenkovich, Matrix approach to Lagrangian fluid dynamics, *J. Fluid Mechanics*, 443 (2001), 167 – 196.

A Pressure equation in the corrector substep

The explicit form of the equation for the pressure $P^{n+1/2}$ at the intermediate step is the following one:

$$(\mathcal{A}\,\partial^2_{\xi\xi} + \mathcal{B}\,\partial^2_{\xi\eta} + \mathcal{C}\,\partial^2_{\eta\eta} + \mathcal{D}\,\partial_\xi + \mathcal{E}\,\partial_\eta)P^{n+1/2} = \mathcal{F}\,,$$

where the coefficients are:

$$\begin{aligned}
\mathcal{A} &= \Delta t\,[|\boldsymbol{x}_\eta^{n+1/2}|^2 + \Delta t_2\,\boldsymbol{x}_\eta^{n+1/2}\cdot(2\boldsymbol{u}_\eta^{n+1/2} - \boldsymbol{u}_\eta^n)] \\
\mathcal{B} &= -\Delta t\,\{2\,\boldsymbol{x}_\xi^{n+1/2}\cdot\boldsymbol{x}_\eta^{n+1/2} + \\
&\quad +\Delta t_2\,[\boldsymbol{x}_\xi^{n+1/2}\cdot(2\boldsymbol{u}_\eta^{n+1/2} - \boldsymbol{u}_\eta^n) + \boldsymbol{x}_\eta^{n+1/2}\cdot(2\boldsymbol{u}_\xi^{n+1/2} - \boldsymbol{u}_\xi^n)]\} \\
\mathcal{C} &= \Delta t\,[|\boldsymbol{x}_\xi^{n+1/2}|^2 + \Delta t_2\,\boldsymbol{x}_\xi^{n+1/2}\cdot(2\boldsymbol{u}_\xi^{n+1/2} - \boldsymbol{u}_\xi^n)] \\
\mathcal{D} &= \Delta t\,\{\boldsymbol{x}_{\xi\eta}^{n+1/2}\cdot\boldsymbol{x}_\eta^{n+1/2} - \boldsymbol{x}_{\eta\eta}^{n+1/2}\cdot\boldsymbol{x}_\xi^{n+1/2} + \\
&\quad +\Delta t_2\,[\boldsymbol{x}_{\xi\eta}^{n+1/2}\cdot(2\boldsymbol{u}_\eta^{n+1/2} - \boldsymbol{u}_\eta^n) - \boldsymbol{x}_{\eta\eta}^{n+1/2}\cdot(2\boldsymbol{u}_\xi^{n+1/2} - \boldsymbol{u}_\xi^n)]\} \\
\mathcal{E} &= \Delta t\,\{\boldsymbol{x}_{\xi\eta}^{n+1/2}\cdot\boldsymbol{x}_\xi^{n+1/2} - \boldsymbol{x}_{\xi\xi}^{n+1/2}\cdot\boldsymbol{x}_\eta^{n+1/2} + \\
&\quad +\Delta t_2\,[\boldsymbol{x}_{\xi\eta}^{n+1/2}\cdot(2\boldsymbol{u}_\xi^{n+1/2} - \boldsymbol{u}_\xi^n) - \boldsymbol{x}_{\xi\xi}^{n+1/2}\cdot(2\boldsymbol{u}_\eta^{n+1/2} - \boldsymbol{u}_\eta^n)]\} \\
\mathcal{F} &= \Delta t\,(u_\xi^{n+1/2}v_\eta^n - u_\eta^{n+1/2}v_\xi^n + u_\xi^n v_\eta^{n+1/2} - u_\eta^n v_\xi^{n+1/2}) + \\
&\quad +(y_\eta^n u_\xi^n - y_\xi^n u_\eta^n - x_\eta^n v_\xi^n + x_\xi^n v_\eta^n)\,.
\end{aligned}$$

It is worth observing that the second contribution in the definition of the coefficient $\mathcal{F}$ is just the divergence of the velocity $\boldsymbol{u}^n$, *i.e.* $(\boldsymbol{G}_n^{-1}\cdot\boldsymbol{\nabla})\cdot\boldsymbol{u}^n$.

B Second order expansion for the flow

In the present appendix some technical details about the second order expansion, summarized in Section 4, are given for the reader convenience.

The coefficients resulting from the integral of $\Pi_{rq}(\eta;t)$ times $\cosh \mathrm{M}\eta$ ($\boldsymbol{C}$) or $\sinh \mathrm{M}\eta$ ($\boldsymbol{S}$) in η are the following ones:

$$
\begin{aligned}
\boldsymbol{C}^{(1)}_{rq,m}(\eta) &= 2\mathrm{i}\mathrm{Q}\left\{ \mathrm{M}[\boldsymbol{s}^{uv}_{rq,m}(\eta) - \mathrm{i}\boldsymbol{c}^{uu}_{rq,m}(\eta)] - \boldsymbol{U}_r(\eta)\boldsymbol{V}_q(\eta)\cosh \mathrm{M}\eta \right\}\\
\boldsymbol{S}^{(1)}_{rq,m}(\eta) &= 2\mathrm{i}\mathrm{Q}\left\{ \mathrm{M}[\boldsymbol{c}^{uv}_{rq,m}(\eta) - \mathrm{i}\boldsymbol{s}^{uu}_{rq,m}(\eta)] - \boldsymbol{U}_r(\eta)\boldsymbol{V}_q(\eta)\sinh \mathrm{M}\eta \right\}\\
\boldsymbol{C}^{(2)}_{rq,m}(\eta) &= \frac{\nu_q \boldsymbol{V}_q(h)}{\sinh \mathrm{Q}h}\left\{ -\frac{\boldsymbol{V}_r(h)}{\sinh \mathrm{R}h}\left(\mathrm{Q}\sinh 2\mathrm{R}\eta + \mathrm{R}\sinh 2\mathrm{Q}\eta\right) + \right.\\
&\qquad +\mathrm{i}\left[\boldsymbol{U}_{r,\eta}(\eta)\cosh \mathrm{Q}\eta\cosh \mathrm{M}\eta - \boldsymbol{U}_{r,\eta}(0) + \right.\\
&\qquad\quad \left. -\frac{1}{2}\left(\mathrm{R}\sinh(\mathrm{M}+\mathrm{Q})\eta + (\mathrm{M}+\mathrm{Q})\sinh \mathrm{R}\eta\right)\boldsymbol{U}_r(\eta)\right] +\\
&\qquad +\left[\boldsymbol{V}_{r,\eta}(\eta)\sinh \mathrm{Q}\eta\cosh \mathrm{M}\eta + \right.\\
&\qquad\quad \left.\left. +\frac{1}{2}\left((\mathrm{M}+\mathrm{Q})\cosh \mathrm{R}\eta - \mathrm{R}\cosh(\mathrm{M}+\mathrm{Q})\eta\right)\boldsymbol{V}_r(\eta)\right]\right\}\\
\boldsymbol{S}^{(2)}_{rq,m}(\eta) &= \frac{\nu_q \boldsymbol{V}_q(h)}{\sinh \mathrm{Q}h}\left\{ -\frac{\boldsymbol{V}_r(h)}{\sinh \mathrm{R}h}\left(\mathrm{Q}\cosh 2\mathrm{R}\eta + \mathrm{R}\cosh 2\mathrm{Q}\eta - \mathrm{Q} - \mathrm{R}\right) + \right.\\
&\qquad +\mathrm{i}\left[\boldsymbol{U}_{r,\eta}(\eta)\cosh \mathrm{Q}\eta\sinh \mathrm{M}\eta + \mathrm{M}\boldsymbol{U}_r(0) + \right.\\
&\qquad\quad \left. -\frac{1}{2}\left(\mathrm{R}\cosh(\mathrm{M}+\mathrm{Q})\eta + (\mathrm{M}+\mathrm{Q})\cosh \mathrm{R}\eta\right)\boldsymbol{U}_r(\eta)\right] +\\
&\qquad +\left[\boldsymbol{V}_{r,\eta}(\eta)\sinh \mathrm{Q}\eta\sinh \mathrm{M}\eta + \right.\\
&\qquad\quad \left.\left. +\frac{1}{2}\left((\mathrm{M}+\mathrm{Q})\sinh \mathrm{R}\eta - \mathrm{R}\sinh(\mathrm{M}+\mathrm{Q})\eta\right)\boldsymbol{V}_r(\eta)\right]\right\}\\
\boldsymbol{C}^{(3)}_{rq,m}(\eta) &= \frac{\nu_q}{\nu_r}\frac{\boldsymbol{V}_r(h)\boldsymbol{V}_q(h)}{\sinh \mathrm{R}h\sinh \mathrm{Q}h}\left(\mathrm{Q}\sinh 2\mathrm{R}\eta + \mathrm{R}\sinh 2\mathrm{Q}\eta\right)\\
\boldsymbol{S}^{(3)}_{rq,m}(\eta) &= \frac{\nu_q}{\nu_r}\frac{\boldsymbol{V}_r(h)\boldsymbol{V}_q(h)}{\sinh \mathrm{R}h\sinh \mathrm{Q}h}\left(\mathrm{Q}\cosh 2\mathrm{R}\eta + \mathrm{R}\cosh 2\mathrm{Q}\eta - \mathrm{Q} - \mathrm{R}\right)\\
\boldsymbol{C}^{(4)}_{rq,m}(\eta) &= -\frac{\mathrm{R}\boldsymbol{V}_r(h)}{(\mathrm{M}+\mathrm{R})\sinh \mathrm{R}h}\left\{ 2\mathrm{i}\mathrm{M}\mathrm{Q}\boldsymbol{c}^{u}_{q,m+r}(\eta) + \right.
\end{aligned}
$$

$$
\begin{aligned}
&\qquad\qquad + \left[\mathrm{Q}\cosh(\mathrm{M}+\mathrm{R})\eta - (\mathrm{M}+\mathrm{R})\cosh \mathrm{Q}\eta \right] \boldsymbol{V}_q(\eta) \Big\} \\
\boldsymbol{S}^{(4)}_{rq,m}(\eta) &= -\frac{\mathrm{R}\boldsymbol{V}_r(h)}{(\mathrm{M}+\mathrm{R})\sinh \mathrm{R}h} \Big\{ 2\mathrm{i}\mathrm{M}\mathrm{Q}\boldsymbol{s}^u_{q,m+r}(\eta) + \\
&\qquad\qquad + \left[\mathrm{Q}\sinh(\mathrm{M}+\mathrm{R})\eta - (\mathrm{M}+\mathrm{R})\sinh \mathrm{Q}\eta \right] \boldsymbol{V}_q(\eta) \Big\} \\
\boldsymbol{C}^{(5)}_{rq,m}(\eta) &= \frac{2\mathrm{i}\mathrm{Q}\boldsymbol{V}_q(h)}{\sinh \mathrm{Q}h} \left[\boldsymbol{U}_r(\eta)\sinh \mathrm{Q}\eta\cosh \mathrm{M}\eta - \mathrm{M}\boldsymbol{c}^u_{r,m+q}(\eta) \right] \\
\boldsymbol{S}^{(5)}_{rq,m}(\eta) &= \frac{2\mathrm{i}\mathrm{Q}\boldsymbol{V}_q(h)}{\sinh \mathrm{Q}h} \left[\boldsymbol{U}_r(\eta)\sinh \mathrm{Q}\eta\sinh \mathrm{M}\eta - \mathrm{M}\boldsymbol{s}^u_{r,m+q}(\eta) \right] \\
\boldsymbol{C}^{(6)}_{rq,m}(\eta) &= -\frac{1}{2}\,\frac{\boldsymbol{V}_r(h)\boldsymbol{V}_q(h)}{\sinh \mathrm{R}h\sinh \mathrm{Q}h} \left(\mathrm{Q}\sinh 2\mathrm{R}\eta + \mathrm{R}\sinh 2\mathrm{Q}\eta\right) \\
\boldsymbol{S}^{(6)}_{rq,m}(\eta) &= -\frac{1}{2}\,\frac{\boldsymbol{V}_r(h)\boldsymbol{V}_q(h)}{\sinh \mathrm{R}h\sinh \mathrm{Q}h} \left(\mathrm{Q}\cosh 2\mathrm{R}\eta + \mathrm{R}\cosh 2\mathrm{Q}\eta - \mathrm{Q} - \mathrm{R}\right) .
\end{aligned}
$$

Another point in which details have been omitted regards the solution of the differential problem (26) for Fourier's coefficient $\boldsymbol{y}^{(2)}_m(h;t)$. Here, the integration in τ of the forcing term $\boldsymbol{T}(\tau)$ (27) times the kernel $\sin\nu_m(t-\tau)$ is needed. To this aim, the following integrals have to be evaluated:

$$
\begin{aligned}
\mathcal{I}^{(1)}_m(t) &= \int_0^t d\tau\ \sin[\nu_m(t-\tau)] = \frac{1}{\nu_m}\,(1-\cos\nu_m t) \\
\mathcal{I}^{(2)}_{q,m}(t) &= \int_0^t d\tau\,\tau\ \sin\nu_q\tau\ \sin\nu_m(t-\tau) \\
&= \frac{\nu_m}{\nu_m^2-\nu_q^2}\,t\sin\nu_q t + \frac{2\nu_m\nu_q}{(\nu_m^2-\nu_q^2)^2}\,(\cos\nu_m t - \cos\nu_q t) \\
\mathcal{I}^{(3)}_{rq,m}(t) &= \int_0^t d\tau\ \sin\nu_r\tau\ \sin\nu_q\tau\ \sin\nu_m(t-\tau) \\
&= \frac{\nu_m}{2}\left[\,\frac{\cos\nu_m t - \cos(\nu_r+\nu_q)t}{\nu_m^2-(\nu_r+\nu_q)^2} + \frac{\cos(\nu_r-\nu_q)t - \cos\nu_m t}{\nu_m^2-(\nu_r-\nu_q)^2}\,\right] \\
\mathcal{I}^{(4)}_{r,m}(t) &= \int_0^t d\tau\,(1-\cos\nu_r\tau)\ \sin[\nu_m(t-\tau)] \\
&= \frac{\nu_r^2(1-\cos\nu_m t) - \nu_m^2(1-\cos\nu_r t)}{\nu_m(\nu_r^2-\nu_m^2)} \\
\mathcal{I}^{(5)}_{rq,m}(t) &= \int_0^t d\tau\,(1-\cos\nu_r\tau)\,(1-\cos\nu_q\tau)\ \sin\nu_m(t-\tau) \\
&= \frac{1}{\nu_m}\,(1-\cos\nu_m t) + \frac{\nu_m(\cos\nu_m t - \cos\nu_r t)}{\nu_m^2-\nu_r^2} + \\
&\quad + \frac{\nu_m(\cos\nu_m t - \cos\nu_q t)}{\nu_m^2-\nu_q^2} + \frac{\nu_m[\cos(\nu_r+\nu_q)t - \cos\nu_m t]}{2[\nu_m^2-(\nu_r+\nu_q)^2]} +
\end{aligned}
$$

$$+\frac{\nu_m[\cos(\nu_r-\nu_q)t-\cos\nu_m t]}{2[\nu_m^2-(\nu_r-\nu_q)^2]}\,.$$

The secular term proportional to $t\sin\nu_q t$ in $\mathcal{I}^{(2)}_{q,m}$ accounts for the lack of periodicity of the free surface elevation at the second order. Moreover, other time integrals have to be evaluated, in order to compute Fourier's coefficient $\boldsymbol{y}^{(2)}_m(\eta;t)$ for $0<\eta<h$. As a matter of fact, the solution (28) is put into the differential problem (25) for $\boldsymbol{y}^{(2)}_m$ and then it is integrated two times in time, starting from homogeneous conditions on velocity and position. When the terms in $\tilde{\boldsymbol{C}}^{(2,3)}_{rq,m}$ and the two integrals of Π_{Ra} are considered, the following time integrals are required for $r\neq q$:

$$\begin{aligned}
\mathcal{J}^{(1)}_m(t) &= \int_0^t d\tau'\int_0^{\tau'} d\tau''\;\tau''\sin\nu_m\tau'' \\
&= \frac{1}{\nu_m^3}[2\,(1-\cos\nu_m t)-\nu_m t\,\sin\nu_m t] \\
\mathcal{J}^{(2)}_{rq}(t) &= \int_0^t d\tau'\int_0^{\tau'} d\tau''\;\sin\nu_r\tau''\sin\nu_q\tau'' \\
&= \frac{1-\cos(\nu_r-\nu_q)t}{2(\nu_r-\nu_q)^2}-\frac{1-\cos(\nu_r+\nu_q)t}{2(\nu_r+\nu_q)^2} \\
\mathcal{J}^{(3)}_m(t) &= \int_0^t d\tau'\int_0^{\tau'} d\tau''\,(1-\cos\nu_m\tau'')=\frac{1}{\nu_m^2}\left(\cos\nu_m t-1+\frac{1}{2}\,\nu_m^2t^2\right) \\
\mathcal{J}^{(4)}_{rq}(t) &= \int_0^t d\tau'\int_0^{\tau'} d\tau''\,(1-\cos\nu_r\tau'')\,(1-\cos\nu_q\tau'') \\
&= \frac{t^2}{2}-\frac{1-\cos\nu_r t}{\nu_r^2}-\frac{1-\cos\nu_q t}{\nu_q^2}+ \\
&\quad+\frac{1-\cos(\nu_r+\nu_q)t}{2(\nu_r+\nu_q)^2}+\frac{1-\cos(\nu_r-\nu_q)t}{2(\nu_r-\nu_q)^2}\,,
\end{aligned}$$

while, for $r=q$, the integrals $\mathcal{J}^{(2)}_{rq}$ and $\mathcal{J}^{(4)}_{rq}$ become:

$$\begin{aligned}
\mathcal{J}^{(2)}_{rr}(t) &= \frac{1}{8\nu_r^2}\left[\cos(2\nu_r t)-1+2\nu_r^2t^2\right] \\
\mathcal{J}^{(4)}_{rr}(t) &= \frac{1}{8\nu_r^2}\left[16\cos\nu_r t-\cos 2\nu_r t+6\nu_r^2t^2-15\right].
\end{aligned}$$

On the other hand, when the terms in $\boldsymbol{y}^{(2)}_m(h;t)$ (28) are considered, the following integrals for $r\neq q$ are needed:

$$\mathcal{J}^{(5)}_m(t) = \int_0^t d\tau'\int_0^{\tau'} d\tau''\,\mathcal{I}^{(1)}_m(\tau'')=\frac{1}{\nu_m^3}\left(\cos\nu_m t-1+\frac{1}{2}\,\nu_m^2t^2\right)$$

$$
\begin{aligned}
\mathcal{J}^{(6)}_{q,m}(t) &= \int_0^t d\tau' \int_0^{\tau'} d\tau'' \, \mathcal{I}^{(2)}_{q,m}(\tau'') \\
&= \frac{\nu_m[2(1-\cos\nu_q t) - \nu_q t \, \sin\nu_q t]}{\nu_q^3(\nu_m^2-\nu_q^2)} + \\
&\quad + \frac{2[\nu_q^2(1-\cos\nu_m t) - \nu_m^2(1-\cos\nu_q t)]}{\nu_m\nu_q(\nu_m^2-\nu_q^2)^2} \\
\mathcal{J}^{(7)}_{rq,m}(t) &= \int_0^t d\tau' \int_0^{\tau'} d\tau'' \, \mathcal{I}^{(3)}_{rq,m}(\tau'') \\
&= \frac{\nu_m}{2} \left\{ \frac{1}{\nu_m^2-(\nu_r+\nu_q)^2} \left[\frac{1-\cos\nu_m t}{\nu_m^2} - \frac{1-\cos(\nu_r+\nu_q)t}{(\nu_r+\nu_q)^2} \right] + \right. \\
&\quad \left. + \frac{1}{\nu_m^2-(\nu_r-\nu_q)^2} \left[\frac{1-\cos(\nu_r-\nu_q)t}{(\nu_r-\nu_q)^2} - \frac{1-\cos\nu_m t}{\nu_m^2} \right] \right\} \\
\mathcal{J}^{(8)}_{r,m}(t) &= \int_0^t d\tau' \int_0^{\tau'} d\tau'' \, \mathcal{I}^{(4)}_{r,m}(\tau'') \\
&= \frac{1}{\nu_m^3\nu_r^2(\nu_r^2-\nu_m^2)} \left[\nu_m^4(1-\cos\nu_r t) - \nu_r^4(1-\cos\nu_m t) + \right. \\
&\quad \left. + \frac{1}{2} \, \nu_m^2\nu_r^2 \, (\nu_r^2-\nu_m^2) \, t^2 \right] \\
\mathcal{J}^{(9)}_{rq,m}(t) &= \int_0^t d\tau' \int_0^{\tau'} d\tau'' \, \mathcal{I}^{(5)}_{rq,m}(\tau'') \\
&= \frac{1}{\nu_m^3} \left(\cos\nu_m t - 1 + \frac{1}{2} \, \nu_m^2 t^2 \right) + \\
&\quad + \frac{\nu_r^2(1-\cos\nu_m t) - \nu_m^2(1-\cos\nu_r t)}{\nu_m\nu_r^2(\nu_m^2-\nu_r^2)} + \\
&\quad + \frac{\nu_q^2(1-\cos\nu_m t) - \nu_m^2(1-\cos\nu_q t)}{\nu_m\nu_q^2(\nu_m^2-\nu_q^2)} + \\
&\quad + \frac{\nu_m^2 \, [1-\cos(\nu_r+\nu_q)t] - (\nu_r+\nu_q)^2(1-\cos\nu_m t)}{2\nu_m(\nu_r+\nu_q)^2[\nu_m^2-(\nu_r+\nu_q)^2]} + \\
&\quad + \frac{\nu_m^2 \, [1-\cos(\nu_r-\nu_q)t] - (\nu_r-\nu_q)^2(1-\cos\nu_m t)}{2\nu_m(\nu_r-\nu_q)^2[\nu_m^2-(\nu_r-\nu_q)^2]} \, ,
\end{aligned}
$$

while for $r = q$ the integrals $\mathcal{J}^{(7)}_{rq,m}$ and $\mathcal{J}^{(9)}_{rq,m}$ become:

$$
\begin{aligned}
\mathcal{J}^{(7)}_{rr,m}(t) &= \frac{\nu_m}{2} \left[\frac{4\nu_r^2(1-\cos\nu_m t)}{\nu_m^4(\nu_m^2-4\nu_r^2)} - \frac{1-\cos 2\nu_r t}{4\nu_r^2(\nu_m^2-4\nu_r^2)} + \frac{t^2}{2\nu_m^2} \right] \\
\mathcal{J}^{(9)}_{rr,m}(t) &= \frac{3}{4\nu_m} \, t^2 - \frac{6\nu_r^4(1-\cos\nu_m t)}{\nu_m^3(\nu_m^2-\nu_r^2)(\nu_m^2-4\nu_r^2)} +
\end{aligned}
$$

$$-\frac{2\nu_m(1-\cos\nu_r t)}{\nu_r^2(\nu_m^2-\nu_r^2)}+\frac{\nu_m(1-\cos 2\nu_r t)}{8\nu_r^2(\nu_m^2-4\nu_r^2)}\,.$$

Finally, the integrals (23), together with the corresponding ones with $\sinh \mathrm{K}\zeta$ replacing $\cosh \mathrm{K}\zeta$, are specified for the form (8) of the initial velocity field:

$$\begin{aligned}
\boldsymbol{c}^{u}_{\alpha,k} &= -\frac{\mathrm{i}}{\pi}\,\frac{hl}{\beta^2l^2+16k^2h^2}\,\Big[4kh\,\sinh \mathrm{K}\eta\,\cos\Big(\beta\frac{\pi}{2}\frac{\eta}{h}\Big)+\\
&\quad +\beta l\,\cosh \mathrm{K}\eta\,\sin\Big(\beta\frac{\pi}{2}\frac{\eta}{h}\Big)\Big]\\
\boldsymbol{s}^{u}_{\alpha,k} &= -\frac{\mathrm{i}}{\pi}\,\frac{hl}{\beta^2l^2+16k^2h^2}\,\Big[4kh\,\cosh \mathrm{K}\eta\,\cos\Big(\beta\frac{\pi}{2}\frac{\eta}{h}\Big)+\\
&\quad +\beta l\,\sinh \mathrm{K}\eta\,\sin\Big(\beta\frac{\pi}{2}\frac{\eta}{h}\Big)-4kh\Big]\\
\boldsymbol{c}^{uu}_{\alpha\alpha,k} &= -\frac{\sinh \mathrm{K}\eta}{8\mathrm{K}}-\frac{1}{8\pi}\,\frac{hl}{\beta^2l^2+4k^2h^2}\,\Big[2kh\,\sinh \mathrm{K}\eta\,\cos\Big(\pi\beta\frac{\eta}{h}\Big)+\\
&\quad +\beta l\,\cosh \mathrm{K}\eta\,\sin\Big(\pi\beta\frac{\eta}{h}\Big)\Big]\\
\boldsymbol{s}^{uu}_{\alpha\alpha,k} &= -\frac{\cosh \mathrm{K}\eta-1}{8\mathrm{K}}-\frac{1}{8\pi}\,\frac{hl}{\beta^2l^2+4k^2h^2}\,\Big[2kh\,\cosh \mathrm{K}\eta\,\cos\Big(\pi\beta\frac{\eta}{h}\Big)+\\
&\quad +\beta l\,\sinh \mathrm{K}\eta\,\sin\Big(\pi\beta\frac{\eta}{h}\Big)-2kh\Big]\\
\boldsymbol{c}^{uv}_{\alpha\alpha,k} &= -\frac{\mathrm{i}\,\rho}{8\pi}\,\frac{hl}{\beta^2l^2+4k^2h^2}\,\Big[2kh\,\sinh \mathrm{K}\eta\,\sin\Big(\pi\beta\frac{\eta}{h}\Big)+\\
&\quad -\beta l\,\cosh \mathrm{K}\eta\,\cos\Big(\pi\beta\frac{\eta}{h}\Big)+\beta l\Big]\\
\boldsymbol{s}^{uv}_{\alpha\alpha,k} &= -\frac{\mathrm{i}\,\rho}{8\pi}\,\frac{hl}{\beta^2l^2+4k^2h^2}\,\Big[2kh\,\cosh \mathrm{K}\eta\,\sin\Big(\pi\beta\frac{\eta}{h}\Big)+\\
&\quad -\beta l\,\sinh \mathrm{K}\eta\,\cos\Big(\pi\beta\frac{\eta}{h}\Big)\Big]\,.
\end{aligned}$$

Received: April 14, 2008